

# Measurement of the differential and total cross-sections of $\gamma$ -ray emission induced by 14.1 MeV neutrons for C, Al, Si, Ca, Ti, Cr, and Fe using the tagged neutron method\*

P.S. Prusachenko<sup>1†</sup> D.N. Grozdanov<sup>1,2</sup> N.A. Fedorov<sup>1</sup> Yu.N. Kopatch<sup>1</sup> G.V. Pampushik<sup>1,3</sup> P.I. Kharlamov<sup>1,3,4</sup>  
V.R. Skoy<sup>1</sup> I.N. Ruskov<sup>1,2</sup> T.Yu. Tretyakova<sup>1,3,4</sup> A.V. Andreev<sup>1,3</sup> C. Hramco<sup>1</sup> P.G. Filonchik<sup>1,5</sup>

TANGRA collaboration

<sup>1</sup>Joint Institute for Nuclear Research (JINR), Dubna, Russia

<sup>2</sup>Institute for Nuclear Research and Nuclear Energy, Bulgarian Academy of Sciences, Sofia, Bulgaria

<sup>3</sup>Faculty of Physics, Lomonosov Moscow State University, Moscow, Russia

<sup>4</sup>Skobeltsyn Institute of Nuclear Physics, Moscow State University, Moscow, Russia

<sup>5</sup>Moscow Institute of Physics and Technology, Moscow, Russia

**Abstract:** In this work, differential cross sections of  $\gamma$ -ray emission produced in nuclear reactions induced by 14.1 MeV neutrons are measured for the 4.439 MeV line from carbon, as well as for 10 individual  $\gamma$ -ray lines from aluminum, 6 from silicon, 8 from calcium, 16 from titanium, 6 from chromium, and 14 from iron. The measurements were conducted using the tagged neutron method with four LaBr<sub>3</sub>(Ce) scintillation detectors positioned at angles of 25°, 45°, 60°, and 70° relative to the generator target – sample center axis. A neutron generator capable of producing 16 separate beams of tagged neutrons was employed, which, combined with the detector system, enabled the determination of differential cross-sections for 64 distinct angle values in the range of 17° to 89°. To simplify data visualization, the angular distributions were divided into 5° intervals, with weighted mean values of the angle and differential cross-section calculated for each interval. Corrections for multiple neutron scattering and attenuation,  $\gamma$ -ray attenuation, and total detection efficiency, computed using GEANT4, were accounted for in the cross-section calculations. Additional measurements were performed to validate the correction calculations. The total  $\gamma$ -ray emission cross-sections were obtained by approximating the angular distributions with even-order Legendre polynomial expansions up to the 6th degree, followed by integration over the full solid angle. The total systematic error for the obtained data was estimated as 9.1%.

**Keywords:** tagged neutron method, differential and total  $\gamma$ -ray production cross sections, 14.1 MeV neutrons

**DOI:**      **CSTR:**

## I. INTRODUCTION

The study of characteristic  $\gamma$ -ray emission in nuclear reactions induced by fast neutrons is of significant interest for a range of fundamental and applied problems. In particular, it provides additional information about nuclear structure and the probability of exciting specific nuclear states. Spectroscopy of characteristic  $\gamma$ -rays emitted in reactions induced by fast neutrons (most commonly with energies around 14 MeV) is frequently used to investigate the elemental composition of various materials [1]. However, it is noted that the accuracy of existing experimental and evaluated data on  $\gamma$ -ray emission under fast neutron irradiation requires substantial im-

provement to meet modern demands and support emerging fields such as planetary nuclear spectroscopy.

The TANGRA (TAGged Neutrons and Gamma-RAYS) project at the Frank Laboratory of Neutron Physics, Joint Institute for Nuclear Research (JINR) [2, 3], employs the tagged neutron method (TNM) [4] to address current fundamental and applied challenges [5]. The tagged neutron method offers a simple and cost-effective alternative to pulsed neutron generators while retaining many of their advantages (e.g., time-of-flight background suppression, compactness, etc.). Due to these benefits, TNM has been applied to various practical problems, including geology [6], metallurgy [7], and hazardous material detection [8]. To enhance the accuracy of

Received 28 August 2025; Accepted 6 November 2025

\* This work was supported by a RSF grant No.23-12-00239

† E-mail: prusachenko@jinr.ru

©2026 Chinese Physical Society and the Institute of High Energy Physics of the Chinese Academy of Sciences and the Institute of Modern Physics of the Chinese Academy of Sciences and IOP Publishing Ltd. All rights, including for text and data mining, AI training, and similar technologies, are reserved.

analysis and expand its applications, the TANGRA project is conducting a large-scale study of angular distributions and cross-sections for characteristic  $\gamma$ -ray emission induced by 14.1 MeV neutrons across a wide range of elements [9–14]. It is worth noting that the papers [9, 10, 12, 13] presented only relative measurement results, while the paper [14] presented preliminary results that did not take into account corrections for multiple scattering and attenuation of neutrons in the neutron generator. Among the elements of particular interest are carbon, aluminum, silicon, calcium, titanium, chromium, and iron, which are major constituents of many geological materials and some hazardous substances.

Currently, a considerable amount of experimental data exists for these elements at neutron energies near 14 MeV, particularly for carbon [15–27, 27–38], aluminum [15, 24, 28, 31, 39–46], silicon [19, 26, 28, 30, 42, 47–58], calcium [19], titanium [19, 31, 49, 51, 53, 59–64], chromium [39, 49, 50, 59, 60, 65–69], and iron [26, 30, 46, 47, 49, 52, 53, 59, 65, 67, 70–84]. Despite the impressive number of studies, one of the major issues is the fragmented and insufficient data on angular distributions of  $\gamma$ -rays emitted in neutron-induced reactions. According to Simakov's compilation [85], which provides a detailed review of experimental data available up to 1998 (see Table 3 in [85]), most measurements were performed for only 1–2 angular points, making it impossible to accurately assess  $\gamma$ -ray emission anisotropy or reliably estimate total cross-sections. Additionally, many studies lack detailed descriptions of experimental setups and data correction methodologies, complicating efforts to resolve discrepancies in reported cross-sections. Some recent studies, such as those conducted at the GAINS setup in GELINA [57, 64, 79], provide thorough descriptions of experimental procedures and data analysis. However, their limitations include a narrow selection of studied elements and the absence of angular distribution measurements.

The objective of this research was to perform more precise and detailed measurements of differential  $\gamma$ -ray emission cross-sections for the most intense transitions in carbon, aluminum, silicon, calcium, titanium, chromium, and iron nuclei under irradiation by 14.1 MeV neutrons, followed by the determination of total cross-sections. The detector and sample geometry, as well as sample dimensions, were optimized to minimize some systematic uncertainties, such as incomplete sample coverage by tagged neutron beams.

## II. EXPERIMENT

The tagged neutron method is based on the detection of secondary  $\alpha$ -particles accompanying neutron emission in the  ${}^3\text{H}(d,n){}^4\text{He}$  fusion reaction using a position-sensitive charged particle detector integrated into the neutron

generator vacuum chamber. This provides information about the neutron emission time, direction, and its flux. A characteristic feature of this method is the relatively large size of the tagged neutron beam field, which necessitates either using large samples or accepting that not all neutrons in the beam will hit the sample surface. This can introduce significant systematic effects that distort measurement results, including uncertainty in determining the number of neutrons incident on the sample, as well as absorption and multiple scattering of both  $\gamma$ -rays and neutrons in the sample. In this work, the geometric parameters of the setup were optimized to minimize some of these effects. In particular, the sample size was selected to ensure complete interception of all tagged neutron beams, while the thickness was reduced compared to previous experiments in the TANGRA project. A series of additional experiments were conducted to evaluate the accuracy of correction factors and measurement uncertainty limits.

The general layout of the experimental setup is shown in Fig. 1. The neutron source was an ING-27 generator [86] with accelerated deuteron energies of 30 – 90 keV. The  $\alpha$ -particles accompanying neutron emission were detected using a built-in position-sensitive charged particle detector. This detector consists of 16 vertical and 16 horizontal strips forming 256 pixels. Each pixel size was  $4 \times 4$  mm<sup>2</sup>, and the distance between the tritium target and  $\alpha$ -particle detector was 44 mm. In this work, to increase counting statistics, data from only 16 vertical strips were

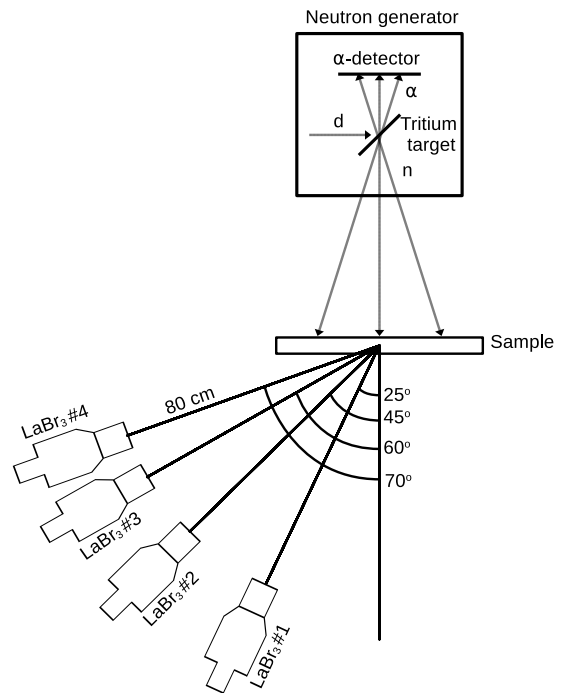


**Fig. 1.** Layout of the experimental setup (not to scale).  $d$ ,  $n$ ,  $\alpha$  – designations of deuteron beams, tagged neutrons and  $\alpha$ -particles, respectively.

used without pixel subdivision. According to the neutron generator documentation, the distance between individual strips (the dead zone) was 0.1 mm. A separate examination of crosstalk between adjacent strips of the neutron generator was performed. For this purpose, an additional analysis of the measurement results with a  $\text{TiO}_2$  sample was conducted. In this analysis, in addition to the " $\alpha$ - $\gamma$ " coincidences for a specific strip, events corresponding to the coincidence of signals from two adjacent strips and  $\gamma$ -rays corresponding to an energy of 983 keV (the most intense line emitted during the interaction of 14.1 MeV neutrons with titanium nuclei) were also selected. The selection criterion for such events was a time difference between signals from adjacent strips of less than 10 ns. The fraction of events satisfying this criterion was  $4 \pm 1\%$ . It should be noted that this figure includes not only "true" crosstalk events, but also, to a significant extent, the "electronic" events associated with signal interference in the cable connecting the  $\alpha$ -detector preamplifier and the digitizer. A correction for crosstalk was made during data analysis, and the uncertainty in this value was taken into account when analyzing the total measurement uncertainty.

The detection efficiency for the  $\alpha$ -particle detector is about 90%. However, the loss of  $\alpha$ -particles does not distort the measurement results. The absolute flux of the tagged neutron beam was determined directly from the measured  $\alpha$ -particle count rate. Neutrons whose associated  $\alpha$ -particles are not detected are excluded from the defined beam and their interactions form part of the untagged background, which is determined from the random coincidence region of the time-of-flight spectra and subtracted. Therefore, the  $\alpha$ -detection efficiency is inherent to the flux definition and does not require a separate correction for normalization. A more detailed description of the neutron generator used is provided in [86].

The experiment utilized samples of graphite, silicon and chromium oxides, as well as metallic aluminum, titanium and iron with natural isotopic abundance. Each sample measured  $44 \times 44 \text{ cm}^2$ , a size selected to ensure complete interception of all tagged neutron beams at the chosen target-to-sample distance of 24.8 cm. The mass of each sample was precisely measured using precision electronic scales. Sample thickness ranged from 0.7 to 2 cm. Powdered materials ( $\text{SiO}_2$ ,  $\text{CaO}$  and  $\text{Cr}_2\text{O}_3$ ) were contained in specially fabricated thin polyethylene boxes (3 mm wall thickness). Detailed specifications for each sample used in the study are provided in Table 1. Thickness uniformity was achieved using 10 special steel spacers evenly spaced across the sample area, preventing deformation of the sample box walls. The possible influence of these spacers was taken into account using background measurements with an empty sample box. Thickness variations were estimated to be no more than 1 mm within a single strip while maintaining the average thick-

**Table 1.** Specifications of the samples used in the current work.

Sample	Dimensions ( $\text{cm}^3$ )	Purity (%)	Mass (g)	Density ( $\text{g}/\text{cm}^3$ )
Graphite (C)	$44 \times 44 \times 2$	99	6670	1.64
Al	$44 \times 44 \times 0.76$	99	3978	2.70
$\text{SiO}_2$	$44 \times 44 \times 2$	99	2418	0.62
Ti	$44 \times 44 \times 0.9$	$> 99.5$	7601	4.36
$\text{Cr}_2\text{O}_3$	$44 \times 44 \times 2$	$> 99$	5161	1.33
Fe	$44 \times 44 \times 0.9$	97	13614	7.81
CaO	$44 \times 44 \times 2$	99	2335	0.60

ness indicated in Table 1. Uniformity filling was additionally ensured by preliminary preparation of the powder in order to remove lumps, as well as periodic compaction during the filling process.

The detector system consisted of 4  $\text{LaBr}_3(\text{Ce})$  scintillation detectors with crystal dimensions of  $3'' \times 3''$ . The detectors were positioned at equal distances (80 cm) from the sample center in the horizontal plane at angles of  $25^\circ$ ,  $45^\circ$ ,  $60^\circ$ , and  $70^\circ$  relative to the axis connecting the generator target and the sample center. The combination of 16 vertical  $\alpha$ -detector strips and 4  $\gamma$ -detectors allowed obtaining 64  $\gamma$ -ray emission angles in the range from  $17^\circ$  to  $89^\circ$ . The weighted average  $\gamma$ -ray emission angle and neutron incidence angle were determined by Monte Carlo simulations for each detector-strip combination.

The experimental procedure included separate measurements with each sample, as well as measurements without a sample and with an empty container (for  $\text{SiO}_2$ ,  $\text{CaO}$  and  $\text{Cr}_2\text{O}_3$  samples) to account for time-of-flight dependent background. The core of the data acquisition system was a 128-channel waveform digitizer with a sampling rate of 100 MSamples/sec and 16-bit analog-to-digital converter (ADC) resolution. Signals from each  $\alpha$ -detector strip and each scintillation detector were digitized. At the digital signal processing stage, the main characteristics of each signal were determined, including its time-stamp, amplitude, and pulse area, which is proportional to the light output in the case of scintillation detectors. Then, from the entire event array, coincidences between signals from the  $\alpha$ -detector and  $\gamma$ -ray detectors were selected, and subsequently time and amplitude distributions were constructed for each detector-strip combination. The time-of-flight was estimated as the time difference between signals from the  $\gamma$ -detector and  $\alpha$ -detector. The obtained spectra served as the basis for subsequent processing.

Measurements with each sample under investigation lasted approximately 24 hours. An additional experiment was conducted to estimate potential loss of events due to pulse pileups and dead time at count rates close to the experimental ones (4000-7000 events per second). A  $^{60}\text{Co}$

$\gamma$ -ray source was placed near each  $\text{LaBr}_3\text{:Ce}$  detector such that the count rate did not exceed the background by more than a factor of 1.5. Two sequential measurements were then performed for each detector. In the first, the  $^{60}\text{Co}$  spectrum was measured alone, and then with an additional PuBe source placed close to the detector to raise the total count rate to at least 10000 events per second - exceeding the maximum rate encountered during the actual measurements. Then, from the measured spectra, the area of the full-energy absorption peaks for the 1173 and 1332 keV ( $^{60}\text{Co}$ ) lines were obtained. The fraction of lost events was estimated as the relative difference between the peak areas obtained in measurements with and without the PuBe source, over the same time period. The contribution of such events was less than 1%, which was comparable to the statistical uncertainty of the peak area determination.

The contribution of pileups for the  $\alpha$ -detector under the experimental conditions was no more than 2%, and their influence was additionally suppressed using an upper amplitude threshold. At the same time, dead time in the  $\alpha$ -channels did not significantly distort the results, as a reduction in registered  $\alpha$ -particles led to a corresponding decrease in both the tagged neutron flux and the coincident  $\gamma$ -rays.

### III. DATA ANALYSIS

#### A. Analysis of spectra

Examples of one-dimensional time-of-flight (TOF) distributions for measurements with a titanium sample and without a sample are shown in Fig. 2.

As can be seen from the figure, the spectrum corresponding to the measurement with the sample shows three groups of events, which can be separated by TOF. The

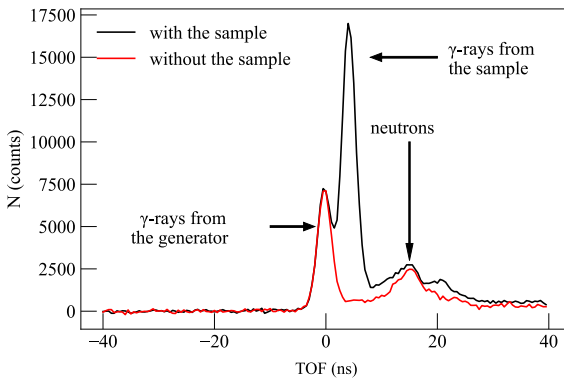


**Fig. 2.** (color online) An example of one-dimensional TOF distributions for measurements with and without a titanium sample, corresponding to the combination "first strip – first detector" (scattering angle  $54^\circ$ ). The TOF distributions are shown after a channel-by-channel subtraction of random coincidences.

first group corresponds to the emission of prompt  $\gamma$ -rays from reactions induced by fast neutrons in the tritium target surroundings (substrate and generator housing), the second group corresponds to the detection of  $\gamma$ -rays resulting from reactions in the sample, and the third group corresponds to neutrons scattered in the sample and generator that hit the gamma detector. In the case of measurements without a sample, only two groups of events are observed, corresponding to prompt  $\gamma$ -rays from the generator and scattered neutrons. At the first stage of spectrum analysis, the random coincidence background was subtracted for all detector-strip combinations. For this purpose, an amplitude spectrum was built in the TOF window corresponding to  $\pm 3\sigma$  from the sample peak position, from which the random coincidence amplitude spectrum constructed in the window from -250 ns to -50 ns was subtracted, taking into account the time window width. This procedure was performed both for spectra obtained from measurements with and without the sample. At the next stage, one-dimensional amplitude spectra were constructed for the same time windows for measurements with the sample and corresponding measurements without the sample. Examples of such spectra are shown in Fig. 3. The background amplitude spectra were subtracted from the spectra measured with the sample, taking into account the difference in the number of registered  $\alpha$ -particles and the effect of shielding the  $\gamma$ -background from the generator by the sample. The latter was estimated by GEANT4 simulations. Thus, spectra corresponding to the registration of only  $\gamma$ -rays from the sample were obtained.

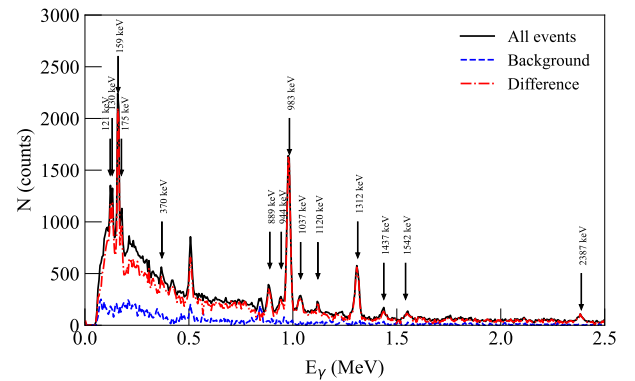


**Fig. 3.** (color online) An example of amplitude spectra before and after background subtraction, corresponding to the combination "first strip – first detector" (scattering angle  $54^\circ$ ). The presented spectra correspond to measurements with the titanium sample, without the sample, and their difference, constructed for the time window of  $\pm 3\sigma$  from the sample peak position on the TOF scale. The amplitude scale is calibrated in units of  $\gamma$ -ray energy. The  $\gamma$ -ray energies shown in the figure correspond to the experimentally observed  $\gamma$ -transitions in titanium nuclei.

After that, the spectra were decoded, full-energy absorption peaks corresponding to the expected transitions in the studied nuclei were identified according to information from the RIPL-3 database [87] and ENSDF [88]. The areas of these peaks were determined from a Gaussian function fit with a linear substrate.

### B. Determination of differential and total cross-sections for individual $\gamma$ -lines

The differential cross-section of  $\gamma$ -ray emission was calculated according to the following expressions:

$$\frac{d\sigma}{d\Omega}(\theta) = \frac{N_p(\theta) \cos \xi}{4\pi N_\alpha n_{nucl} k} \cdot 10^{27} \left[ \frac{\text{mb}}{\text{sr}} \right], \quad (1)$$

$$k = k_{na} \int_0^{x_0} \epsilon(x) k_{ms}(x) k_{\gamma a}(x) dx, \quad (2)$$

where  $N_p$  is the full-energy peak area corresponding to the current detector-strip combination;  $N_\alpha$  is a number of registered  $\alpha$ -particles from the  ${}^3\text{H}(d,n){}^4\text{He}$  reaction for the current strip, corresponding to the number of emitted tagged neutrons;  $n_{nucl}$  is a surface density of nuclei that induced reactions, which lead to formation of the  $\gamma$ -peak;  $\xi$  is an average angle of neutron incidence on the sample for the current strip;  $k$  is an integral correction accounting for attenuation of the tagged neutron beam in the neutron generator  $k_{na}$ , total detection efficiency  $\epsilon$ , contribution of  $\gamma$ -rays resulting from multiple neutron scattering in the sample  $k_{ms}$ , and absorption or energy change of  $\gamma$ -rays due to interactions in the sample  $k_{\gamma a}$ ;  $x_0$  is the sample thickness. The average incidence angle of the primary neutrons varied from  $14^\circ$  for the strip closest to the sample center to  $28^\circ$  for the outermost strips. This resulted in a 10% variation in the effective sample thickness for the central and outer strips. Expression (2) allows proper consideration of changes in total detection efficiency and other corrections depending on the depth  $x$  at which the interaction occurred in the sample. It should be noted that the cross sections obtained in our work are given for  $\gamma$ -lines attributed to a specific isotope or, in cases where the observed peak contains unresolved lines from several isotopes, for the sum of these isotopes. Accordingly, for each observed line, the surface density of nuclei  $n_{nucl}$  in formula (1) was calculated taking into account the abundance of all isotopes of each element whose reactions could contribute to the formation of the studied photopeak:

$$n_{nucl} = \sum_0^I a_i c_i, \quad (3)$$

where  $c$  is the concentration of a specific isotope in the natural mixture on which the reaction occurs producing the target  $\gamma$ -ray line,  $a_i$  is the coefficient representing amount of considered element in the empirical formula of the substance and  $I$  is a number of reaction channels that may contribute to formation of the discussed photopeak.

The correction for absorption of primary neutrons in the target substrate (2 mm copper, tilt angle  $45^\circ$ ) and the neutron generator wall (1.5 mm steel) was calculated in a separate GEANT4 [89, 90] simulation for each strip. The calculation results showed that the number of neutrons reaching the sample decreases by 9% compared to the number emitted, due to absorption and large-angle scattering. Meanwhile, approximately 1.5-2% of the total neutrons reaching the sample have energies below 14 MeV. However, additional calculations demonstrated their negligible contribution to the total yield of emitted  $\gamma$ -rays. The typical values of neutron attenuation in the sample was 4-5% for  $\text{SiO}_2$ , 7-8% for Ti and  $\text{Cr}_2\text{O}_3$  and 11-12% for Fe. It should be noted that the difference in fraction of attenuated neutrons for central and outer strips was about 1% for each sample.

The product of the total  $\gamma$ -ray detection efficiency  $\epsilon$  and the  $\gamma$ -ray attenuation coefficient  $k_{\gamma a}$  as a function of depth in the sample was calculated using the Monte Carlo method in GEANT4 individually for each strip-detector combination. It was determined as the ratio of emitted  $\gamma$ -rays to registered full-energy peak events. A distinctive feature of this procedure was that  $\gamma$ -rays were emitted from the sample region corresponding to a specific strip, while accounting for the decreasing probability of  $\gamma$ -ray emission with increasing depth due to absorption of primary tagged neutrons. To validate the simulation procedure and estimate the associated uncertainties, several additional experiments were performed. The total detection efficiency for  $\gamma$ -rays for a point source was measured using standard  $\gamma$ -ray isotopic sources ( ${}^{22}\text{Na}$ ,  ${}^{60}\text{Co}$ ,  ${}^{137}\text{Cs}$ ,  ${}^{133}\text{Ba}$ ,  ${}^{228}\text{Th}$ ) with known activity (4% uncertainty). The sources were positioned at the center of the Ti sample front plane. The geometry of the sample and detector arrangement was the same as in the main experiment. Using these sources, the detection efficiency was obtained for the  $\gamma$ -ray energy range of 0.08 - 2.614 MeV and subsequently compared with simulation results. The average deviation between the experimental points and the model curve was about 5%, which was close to the uncertainty of the activity of the sources. This value was subsequently used as an estimate of the efficiency uncertainty in the low  $\gamma$ -ray energy region (up to 3.0 MeV), assuming that the uncertainty in the calculated efficiency is the same for a point source and an extended one.

A second experiment measured the relative detection efficiency for high-energy  $\gamma$ -rays. In this setup, a 5-liter container filled with concentrated NaCl solution was placed at the sample position. A  ${}^{239}\text{PuBe}$  neutron source

was inserted to the center of this container. Some neutrons from the source were thermalized and subsequently captured by chlorine nuclei in the solution. Analysis of the measured spectra identified the most intense  $\gamma$ -lines above 3 MeV, corresponding to transitions in  $^{36}\text{Cl}$  nuclei at 7.413, 7.79, and 8.578 MeV (energy values from the prompt  $\gamma$ -ray database [91]). Key selection criteria required these lines to be free from single/double escape peak interference from higher-energy  $\gamma$ -rays. Contributions from  $^{16}\text{O}(n,\gamma)^{17}\text{O}$  and  $^{37}\text{Cl}(n,\gamma)^{38}\text{Cl}$  reactions were considered negligible due to extremely small cross-sections. The 1.951 and 1.959 MeV lines served as reference transitions in the 0.1–3 MeV range where efficiency could be verified using isotopic sources. The relative detection efficiency was then determined using the equation:

$$\epsilon_{\text{relative}}(E) = \frac{N_p(E)k(E)Y(1.951 \text{ MeV})}{N_p(1.951 \text{ MeV})k(1.951 \text{ MeV})Y(E)}, \quad (4)$$

where  $N_p$  is the area of the full-energy peak for the corresponding  $\gamma$ -ray energy,  $k$  is a correction accounting for  $\gamma$ -ray absorption in the source volume, and  $Y$  is a yield for a specific  $\gamma$ -ray line. The yield values and their uncertainties were also taken from the IAEA database [91]. The efficiency values obtained in this way were added to the results of measurements with isotopic sources after normalization. Additional Monte Carlo simulations did not show any significant distortion of the efficiency curve shape between the point source and the PuBe+NaCl volumetric source, meaning that the renormalization performed at approximately 2 MeV allows the two efficiency curves, obtained under different conditions, to be combined. The results of comparing the simulated and experimental efficiency for one of the detectors are shown in Fig. 4. As can be seen from the figure, the simulation results generally agree with the experimental data within the measurement uncertainties. The uncertainty for the high-energy part of the spectrum (above 3 MeV) was estimated by comparing the results of simulations using various sets of electromagnetic physical processes in GEANT4. The maximum difference between them did not exceed 10%, which was accepted as the upper estimate of the efficiency uncertainty in this energy range. It is worth noting that the efficiency obtained using a point source was used only to verify the simulation model, while the final detection efficiency values used in eq. (1)–(2) were obtained from GEANT4 Monte Carlo simulations individually for each detector-strip combination. The calculations took into account the size and spatial position of the region in the sample corresponding to a specific strip from which  $\gamma$ -rays were emitted.

To verify the accuracy of the attenuation coefficient calculation, a series of additional measurements was performed with  $^{137}\text{Cs}$  and  $^{60}\text{Co}$  sources. In these measure-

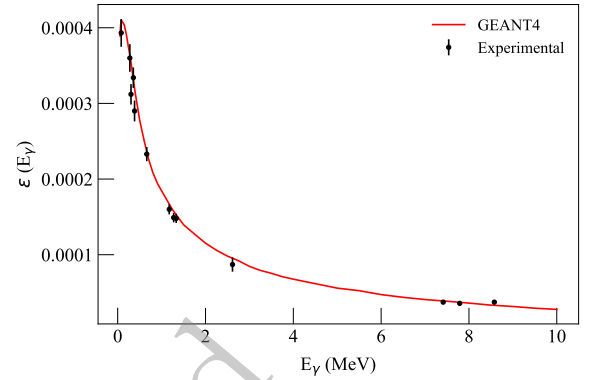


**Fig. 4.** (color online) Comparison of experimental and calculated full-peak detection efficiency for one of the  $\text{LaBr}_3(\text{Ce})$  detectors.

ments, the sources were placed at the center of iron and titanium samples on the side opposite to the detectors. A measurement was also performed with a dummy sample made of thin polystyrene foam, placed in such a way as to maintain the geometry of the detector and source arrangement. The attenuation coefficient for a specific  $\gamma$ -ray line was calculated as the ratio of the full-energy peak area with the sample to the corresponding peak area without the sample. Comparison of the obtained results with GEANT4 simulation results showed that the difference between experiment and calculation does not exceed 2% in all cases. It is worth noting that, despite the relatively narrow energy range, in which the attenuation verification was performed ( $<1.5$  MeV), additional Monte Carlo simulations in GEANT4 showed that the contribution of attenuation in the sample decreases by a factor of 2–3 with increasing energy from 1.5 to 7.0 MeV, which allowed us to accept the obtained contribution to the total error (2%) as the upper limit for the entire energy range.

Separately, a simulation of the coefficient  $k_{ms}$  was performed, which accounted for multiple neutron scattering in the sample with subsequent generation of secondary  $\gamma$ -rays. Direct calculation of this correction in GEANT4 is extremely difficult, primarily due to the inability to account for the influence of  $(n, 2n)$  reactions, since GEANT4 does not model the residual nucleus and its de-excitation for this reaction channel. To partially solve this problem, a two-stage calculation was performed. At the first stage, GEANT4 simulated the transport of neutrons emitted from the generator target through the sample. Here, the sample model was divided into thin layers, and neutron spectra were calculated for each layer. In general, the correction  $k_{ms}$  for  $\gamma$ -rays with the required energy was calculated as the ratio of the calculated number of  $\gamma$ -rays generated by all neutrons  $N_{\gamma}^{\text{tot}}$  to the number generated only by primary neutrons  $N_{\gamma}^i$ , according to the following expression:

$$k_{ms}(x) = \frac{N_{\gamma}^{tot}(x)}{N_{\gamma}^i(x)} = \frac{\sum_0^L \int_0^{14.1} F(E, x) n_j \sigma_j(E) dE}{\sum_0^L F(14.1 \text{ MeV}, x) n_j \sigma_j(14.1 \text{ MeV})}, \quad (5)$$

where  $x$  is the depth in the sample;  $L$  is the number of reaction channels leading to the emission of  $\gamma$ -rays with the required energy;  $F(E, x)$  is the number of neutrons with energy  $E$  at depth  $x$ ;  $\sigma_j(E)$  is the cross-section of  $\gamma$ -ray emission with the required energy induced by neutrons with energy  $E$  for the  $j$ -th reaction channel;  $n_j$  is the surface density of atoms of the isotope on which the  $j$ -th reaction occurs. The energy dependences of the emission cross-sections for the  $\gamma$ -ray energies observed in the experiment were obtained for all possible reaction channels using the TALYS-2.1 code [92] with default parameters. TALYS was chosen due to the opportunity to obtain data on the energy dependence of the  $\gamma$ -ray emission cross section for all lines observed in the experiment, taking into account a large number of excited states and all reaction channels (including  $(n, 2n)$  reactions). Unfortunately, generally accepted libraries of evaluated nuclear data, such as ENDF-B/VIII.0 [93] and JENDL-5 [94], do not provide data on the partial cross sections of  $(n, 2n)$  reactions, which can make a significant contribution to  $\gamma$ -ray production for multi-isotopic elements [95]. A separate issue that should be mentioned is the limited number of states for which partial cross sections of inelastic scattering are provided in standard libraries. This issue can be illustrated using the example of the main isotope of titanium,  $^{48}\text{Ti}$ . Thus, in ENDF-B/VIII.0, partial excitation cross sections are presented for only 18 discrete levels for inelastic scattering on this isotope. The excitation of subsequent states is considered as excitation of a "continuum" with the emission of a continuous  $\gamma$ -ray spectrum. Moreover, for a neutron energy of 14.1 MeV, the total excitation cross section of discrete levels of  $^{48}\text{Ti}$  in inelastic scattering (MT=51-68) is 148 mbarn with a total inelastic scattering cross section of 793 mbarn (MT=4), and the continuum excitation cross section is 645 mbarn (MT=91). The emission cross section of the most intense line with an energy of 983 keV for a neutron energy of 14.1 MeV, calculated on the basis of the data presented in ENDF on the excitation of individual 18 states taking into account cascades (the contribution of which was calculated on the basis of data from MF=12), is 144 mbarn, which is in clear contradiction with the available experimental data on the  $\gamma$ -rays emission cross section with this energy (600-800 mbarn). This information, together with the lack of data on the partial excitation cross sections for individual states of the residual nucleus in the  $(n, 2n)$  reaction does not allow us to assume that the shape of the emission cross section for individual  $\gamma$ -lines can be reproduced using data from standard libraries, in contrast to

calculations using TALYS (see Fig. 5).

Moreover, as can be seen from Fig. 5 using the 983 keV line for titanium as an example, TALYS, in general, allows us to reproduce the shape of the energy dependence of the emission cross section. The difference in magnitude should not introduce a significant uncertainty in the relative calculation of the correction factor using formula (5). It is worth noting separately that in the case of carbon, for which no significant contribution from the  $(n, 2n)$  reaction was expected due to the low content of the  $^{13}\text{C}$  isotope and the high reaction threshold, as well as the absence of a contribution from cascade processes due to the structural features of  $^{12}\text{C}$ , the cross section from ENDF/B-VIII.0 was used as the basis for the calculations. The calculation results showed that the contribution of multiple scattering ranges from 5-10%, depending on the depth in the sample, for lines corresponding to transitions from low-lying states (e.g., 983 keV for titanium or 846 keV for iron) to 15-25% for some individual lines characterized by a very strong dependence of the cross-section on neutron energy, according to TALYS estimates. Fig. 6 demonstrates an example of the total correction factor  $k$  (from Eq. (5)) calculated for specific lines of titanium.

To estimate the uncertainty of the correction factor related to the accuracy of the cross-sections provided by TALYS and ENDF, a separate series of calculations was performed using available experimental data on the energy dependence of emission cross-sections for some  $\gamma$ -lines of C, Si, Ti, and Fe, previously measured at LANL [35] and GELINA [48, 57, 79]. The difference between the cross-sections obtained using TALYS and experi-

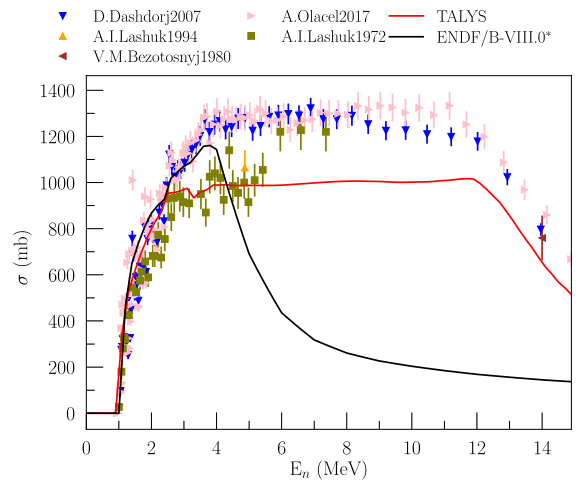


**Fig. 5.** (color online) Emission cross-section for the 983.5 keV  $\gamma$ -line ( $^{48}\text{Ti}(n, n')^{48}\text{Ti}$  and  $^{49}\text{Ti}(n, 2n)^{48}\text{Ti}$  reactions) from TALYS and ENDF/B-VIII.0 as a function of neutron energy in comparison with available experimental data. \*When calculating the cross section from ENDF, only transitions from discrete states were taken into account.

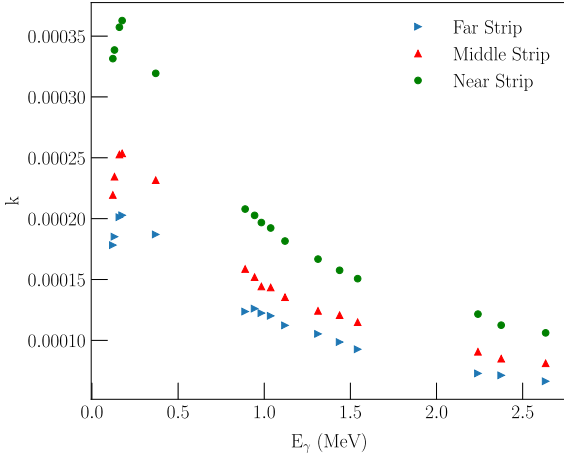


**Fig. 6.** (color online) The total correction factor  $k$  from Eq. (1), calculated for the titanium sample for three combinations of strips (the farthest from the detector strip, the middle, and the nearest strip) with  $\text{LaBr}_3(\text{Ce})$  detector at  $70^\circ$ . The correction values include the full-energy peak detection efficiency, self-absorption, multiple neutron scattering, and neutron attenuation corrections.

mental data was used to estimate the method's uncertainty. Depending on the specific line and element, the contribution of this error was 3-7%, with 7% adopted as the upper uncertainty estimate for all lines.

To verify the accuracy of the correction calculations, additional measurements of  $\gamma$ -ray emission cross-sections were performed for iron samples of different thicknesses (3 mm and 18 mm), in addition to the 9 mm sample used in the main measurements. Among all the samples used in the measurements, iron has the highest effective  $Z$  and density, leading to the largest expected influence of neutron multiple scattering and  $\gamma$ -ray attenuation. The maximum difference between the cross-sections of the same  $\gamma$ -lines obtained for the thinnest and thickest samples did not exceed 7%, which is within the estimated systematic error of this experiment (9%, see Section 3.3).

To obtain the total cross-section, the corresponding differential cross-sections calculated using formula (1) were approximated in the form of a Legendre-polynomial expansion of even order [96]:

$$\frac{d\sigma}{d\Omega}(\theta) = \frac{\sigma_\gamma}{4\pi} \sum_{\nu=0}^{2J} a_\nu P_\nu(\cos\theta). \quad (6)$$

In this expression the coefficient  $a_0$  is equal to 1, and  $J$  is a multipole of the considered  $\gamma$ -transition.

### C. Measurement uncertainties

The main sources of systematic uncertainty in this experiment are given in Table 2.

**Table 2.** Systematic uncertainty budget in the experiment.

Source	Contribution (%)
Efficiency	5 ( $E_\gamma=0-3$ MeV), 10 ( $E_\gamma>3$ MeV)
Correction for attenuation of $\gamma$ -rays in the sample	2
Multiple neutron scattering	7
Crosstalk correction for $\alpha$ -detector	1
Number of nuclei in the sample	2
Total	9.1 ( $E_\gamma=0-3$ MeV), 12.6 ( $E_\gamma>3$ MeV)

The total efficiency uncertainty was estimated as the average difference between efficiency values calculated in GEANT4 and experimental data. The upper limit of uncertainty associated with attenuation of secondary  $\gamma$ -rays in the sample was determined in a separate experiment with  $^{137}\text{Cs}$  and  $^{60}\text{Co}$  sources (see section 3.2). The largest contribution to the systematic uncertainty of this experiment came from the multiple scattering correction in the sample. Its upper limit was estimated by comparing correction coefficients obtained from estimated cross-sections from TALYS code for heavy nuclei (heavier than oxygen), ENDF/B-VIII.0 library for carbon, and available experimental data from literature on energy dependence of emission of individual  $\gamma$ -lines. The uncertainty in the number of nuclei in the sample included both the uncertainty in its mass determination and the uncertainty related to purity of some samples. The total systematic uncertainty was estimated as 9%. The statistical uncertainty for differential cross-sections varied from 0.5-1% for the most intense lines to 20-30% for the least intense lines.

## IV. RESULTS AND DISCUSSION

### A. Carbon

The data on  $\gamma$ -ray emission from the carbon sample are represented solely by the 4.439 MeV line (see Fig. 7 and Table 3), corresponding to the  $2^+ \rightarrow 0^+$  transition in the  $^{12}\text{C}$  nucleus excited via the  $^{12}\text{C}(n,n')^{12}\text{C}$  reaction. The contribution from the  $^{13}\text{C}(n,2n)^{12}\text{C}$  reaction is assumed to be negligible (<1%). As shown in Fig. 7 (a), the angular distribution of 4.439 MeV  $\gamma$ -rays measured in the present work agrees within uncertainties with the data reported in Ref. [34] for angles greater than  $90^\circ$ , as well as with the data from Refs. [19–21, 26, 29, 30, 33], which provide measurements only for angles close to  $90^\circ$ . The differential cross-sections presented in Refs. [16, 22], as well as in Ref. [34] for the angular range of  $0-90^\circ$ , significantly exceed the data obtained in this work, with Ref. [34] exhibiting a notable asymmetry in the angular distribution. Additionally, all experimental angular distributions reported over a wide angular range predict a significant  $a_4$

**Table 3.** Total emission cross-section  $\sigma$  and angular distribution decomposition coefficients into Legendre polynomials  $a_2$  and  $a_4$  for the 4.439 MeV  $\gamma$ -ray line emitted in the interaction of 14.1 MeV neutrons with carbon nuclei. The energies of the initial ( $i$ ) and final ( $f$ ) states are given in MeV.

$E_\gamma$ (MeV)	Reaction	Transition, $E_i (J_i^\pi) \rightarrow E_f (J_f^\pi)$	$\sigma$ (mb)	$a_2$	$a_4$
4.439	$^{12}\text{C}(n,n')^{12}\text{C}$	4.439( $2^+$ ) $\rightarrow$ g.s.( $0^+$ )	$186 \pm 24$	$0.28 \pm 0.01$	$-0.33 \pm 0.02$

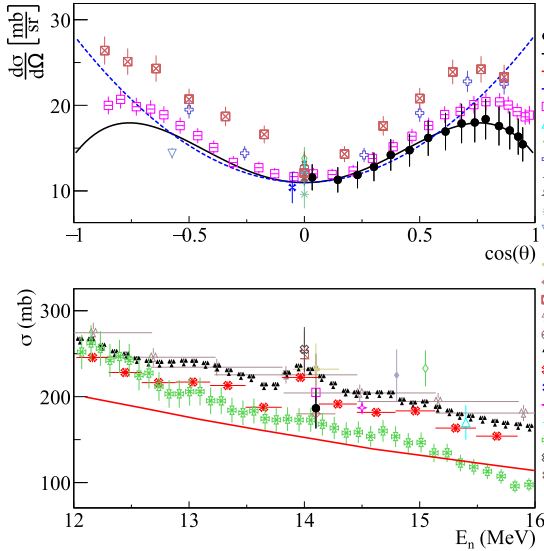


**Fig. 7.** (color online) Differential (a) and total (b) cross sections of  $\gamma$ -ray emission with energy 4.439 MeV from the  $^{12}\text{C}(n,n')^{12}\text{C}$  reaction in comparison with experimental data from other authors, evaluated cross sections from ENDF/B-VIII.0 libraries, and theoretical calculations based on the TALYS program with default parameters. 1 – data from present work; 2 – angular distribution fit from present work using Legendre polynomials; 3 – TALYS calculation; 4 – evaluated cross section from ENDF/B-VIII.0 [93]; 5 – Grozdanov2025 [38]; 6 – Lashuk1994 [31]; 7 – McEvoy2021 [33]; 8 – Spaargaren1971 [22]; 9 – Stewart1964 [17]; 10 – Engesser1967 [19]; 11 – Clayeux1969 [20]; 12 – Morgan1977 [37]; 13 – Morgan1964 [18]; 14 – Kadenko2016 [32]; 15 – Murata1988 [28]; 16 – Benveniste1960 [16]; 17 – Gordon2025 [36]; 18 – Hasegawa1991 [30]; 19, 20 – Kelly2023 [35], direct  $\gamma$ -ray measurement and correlated  $n-\gamma$  measurements; 21 – Zong1979 [26]; 22 – Simakov1998 [85]; 23 – Martin1971 [21]; 24 – Rogers1975 [23]; 25 – Bezotosnyi1975 [24]; 26 – Zhou1989 [29].

coefficient in the Legendre polynomial expansion, whereas the evaluated data from ENDF/B-VIII.0 include only the  $a_2$  coefficient.

As shown in Fig. 7 (b), there is also some discrepancy in the experimental data on total emission cross-sections. Specifically, the total cross-section obtained in this work is noticeably smaller ( $\approx 17\%$ ) than the data from direct  $\gamma$ -ray measurements in Ref. [34] (224 mb), ( $\approx 10\%$ ) larger than the cross-section from Ref. [23] (173 mb), and agrees within uncertainties with the cross-sections

derived from the  $n-\gamma$  correlation experiment in [35], as well as those reported in Ref. [36] and the evaluated cross-section from the ENDF/B-VIII.0 library [93] (210 mb). The cross-section values obtained in a recent experiment within the TANGRA project [38] using an array of plastic scintillation detectors are also consistent with the results presented here, both for the case where the cross-section was determined from the  $\gamma$ -ray angular distribution ( $205 \pm 11$  mb) and for the case where neutrons corresponding to the same scattering channel were detected ( $192 \pm 10$  mb). However, there is a slight difference in the Legendre polynomial expansion coefficients, though it remains within the uncertainties reported in [38]. It is worth noting separately that the results presented in [35], both for the direct measurement of the  $\gamma$ -ray emission cross-section and for the  $n-\gamma$  correlation experiment, represent relative measurements of the energy dependence of the cross-section, normalized to the ENDF/B-VIII.0 evaluated cross-section.

## B. Aluminum and Silicon

The measurement results for the most intense  $\gamma$ -ray lines emitted during the interaction of 14.1 MeV neutrons with silicon and aluminum nuclei are presented in Figs. 8 – 11 and Table 4 and 5.

For the aluminum sample, angular distributions and total emission cross-sections were obtained for  $\gamma$ -ray lines with energies of 0.091, 0.792, 0.843, 0.984, 1.014, 1.698, 1.808, 2.212, 2.298, 3.004 MeV, generated in the reactions  $^{27}\text{Al}(n,n')^{27}\text{Al}$ ,  $^{27}\text{Al}(n,\alpha)^{24}\text{Na}$ ,  $^{27}\text{Al}(n,p)^{27}\text{Mg}$ ,  $^{27}\text{Al}(n,d)^{26}\text{Mg}$ . It should be noted that the available literature data on differential cross-sections for the above lines [19, 20, 26, 30, 59, 65, 72] are extremely fragmentary and mostly limited to 1-2 angular data-points. Data on the total emission cross-sections of these lines are also limited to a small number of studies [24, 28, 31, 39, 41, 42], which show significant scatter, reaching in some cases 30-50% (see Figs. 8 and 9).

For silicon, data on angular distributions and total emission cross-sections were obtained for  $\gamma$ -ray lines with energies of 0.389, 0.585, 1.622, 1.779, 2.271, 2.839 MeV, generated in the reactions  $^{28}\text{Si}(n,p)^{28}\text{Al}$ ,  $^{28}\text{Si}(n,\alpha)^{25}\text{Mg}$ ,  $^{28}\text{Si}(n,n')^{28}\text{Si}$ , and  $^{29}\text{Si}(n,2n)^{28}\text{Si}$ . It should be noted that the excitation of the  $^{28}\text{Si}$  with subsequent emission of the  $\gamma$ -ray with an energy of 1.779 MeV occurs in the both reactions  $^{28}\text{Si}(n,n')^{28}\text{Si}$ , and  $^{29}\text{Si}(n,2n)^{28}\text{Si}$ .

Data for the most intense lines corresponding to the

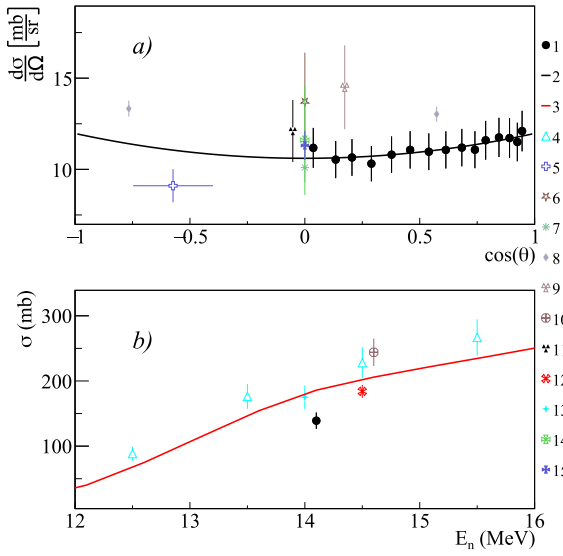


**Fig. 8.** (color online) Differential (a) and total (b) cross-sections of 1.808 MeV  $\gamma$ -ray emission from the  $^{27}\text{Al}(n,d)^{26}\text{Mg}$  reaction, compared with experimental data from other authors and theoretical calculations using the TALYS code with default parameters. 1 – present work data; 2 – Legendre polynomial fit of angular angular distribution from present work; 3 – TALYS calculation; 4 – Pavlik1998 [41]; 5 – Hoot1975 [43]; 6 – Engesser1967 [19]; 7 – Clayeux1969 [20]; 8 – Zhou1997 [44]; 9 – Nyberg1971 [45]; 10 – Hlavac1999 [42]; 11 – Zong1979 [26]; 12 – Simakov1998 [85]; 13 – Bezotosnyi1975 [24]; 14 – Bochkarev1965 [40]; 15 – Hongyu1986 [46].

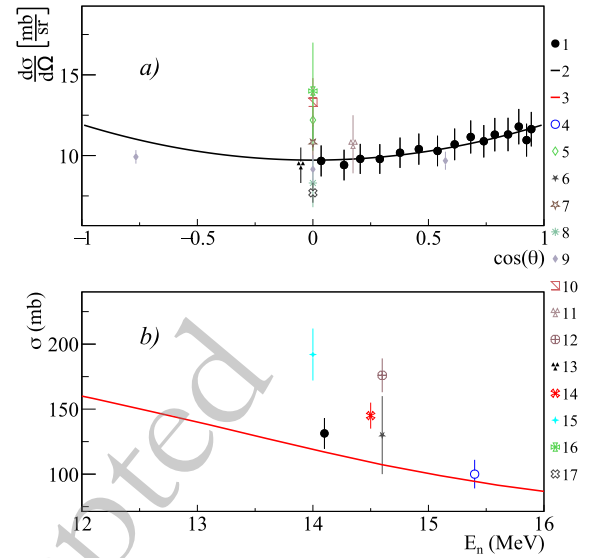


**Fig. 9.** (color online) Differential (a) and total (b) cross-sections of 2.212 MeV  $\gamma$ -ray emission from the  $^{27}\text{Al}(n,n')^{27}\text{Al}$  reaction, compared with experimental data from other authors and theoretical calculations using the TALYS code with default parameters. 1 – present work data; 2 – Legendre polynomial fit of angular angular distribution from present work; 3 – TALYS calculation; 4 – Lashuk1994 [31]; 5 – Sukhanov1970 [72]; 6 – Burymov1969 [39]; 7 – Engesser1967 [19]; 8 – Clayeux1969 [20]; 9 – Zhou1997 [44]; 10 – Hasegawa1991 [30]; 11 – Nyberg1971 [45]; 12 – Hlavac1999 [42]; 13 – Zong1979 [26]; 14 – Simakov1998 [85]; 15 – Bezotosnyi1975 [24]; 16 – Bochkarev1965 [40]; 17 – Hongyu1986 [46].

transitions  $1.779(2^+) \rightarrow \text{g.s.}(0^+)$  and  $4.617(4^+) \rightarrow 1.779(2^+)$  in the  $^{28}\text{Si}$  nucleus are presented in Figs. 10 and 11 in comparison with data from the literature [28, 42, 48, 49, 51, 53–58]. As can be seen from the figures, the data from the present work for these lines agree with the data from other authors within the measurement uncertainties, both for angular distributions and total cross-sections. The results presented for silicon in the previous work within the TANGRA project [14] differ somewhat from the results presented in this work.

It should be noted that the data from [14] were preliminary, as the cross-section calculation did not account for corrections for neutron multiple scattering and neutron attenuation in the generator wall. At the same time, only statistical uncertainty was considered in the error calculation in [14].

Analysis of the measured angular distributions showed a significant contribution from the Legendre polynomial expansion coefficients  $a_2$  and  $a_4$  for the 1.779 MeV line (transition  $1.779(2^+) \rightarrow \text{g.s.}(0^+)$  in the  $^{28}\text{Si}$  nucleus). For the 1.622 and 2.839 MeV lines (transitions  $1.622(2^+) \rightarrow \text{g.s.}(3^+)$  in the  $^{28}\text{Al}$  nucleus and  $4.617(4^+) \rightarrow 1.779(2^+)$  in the  $^{28}\text{Si}$  nucleus), the contribution of the  $a_2$  coefficient is negligible, while the  $a_4$  coefficient is significant. For transitions in the  $^{25}\text{Mg}$  nucleus

( $0.974(3/2^+) \rightarrow 0.585(1/2^+)$  and  $0.585(1/2^+) \rightarrow \text{g.s.}(5/2^+)$ ), the errors in the coefficients were comparable to their magnitudes due to the large statistical scatter in the data.

### C. Calcium and Titanium

The measurement results for the most intense  $\gamma$ -ray lines emitted during the interaction of 14.1 MeV neutrons with calcium and titanium nuclei are presented in Figures 12–15 and in Table 6 and 7.

In the case of calcium, it should be noted that nearly all available experimental data are limited to measurements at  $90^\circ$  (see, for example, [19]), and there are no reliable data whatsoever on total emission cross-sections or angular distributions. In the present work, detailed angular distributions were obtained for the first time for lines with energies of 0.770, 0.891, 2.814, 3.736, and 3.904 MeV, and their total emission cross-sections were determined (see Table 6). The results for the most intense lines 0.891 and 3.736 MeV, are shown in Figure 12 and 13.

Analysis of the measured angular distributions revealed a significant contribution from the first three even-order Legendre polynomial expansion coefficients  $a_2$ ,  $a_4$ , and  $a_6$  for the 2.814 and 3.736 MeV lines, which corres-

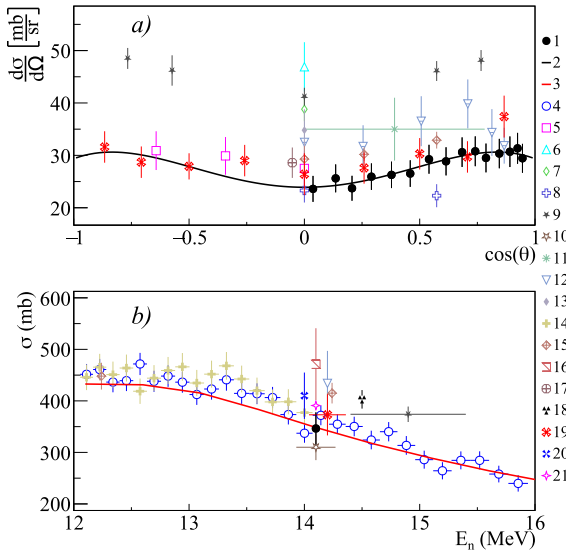


**Fig. 10.** (color online) Differential (a) and total (b) cross-sections of 1.779 MeV  $\gamma$ -ray emission from the  $^{28}\text{Si}(n,n')^{28}\text{Si}$  and  $^{29}\text{Si}(n,2n)^{28}\text{Si}$  reactions, compared with experimental data from other authors and theoretical calculations using the TALYS code with default parameters. 1 – present work data; 2 – Legendre polynomial fit of angular distribution from present work; 3 – TALYS calculation; 4 – Negret2013 [57]; 5 – Drake1978 [52]; 6 – Engesser1967 [19]; 7 – Guoying1992 [54]; 8 – Grenier1974 [50]; 9 – Zhou2011 [56]; 10 – Murata1988 [28]; 11 – Prud'homme1960 [47]; 12 – Connell1975 [51]; 13 – Hasegawa1991 [30]; 14 – Boromiza2020 [58]; 15 – Drosz2002 [55]; 16 – Martin1965 [48]; 17 – Zong1979 [26]; 18 – Simakov1998 [85]; 19 – Abbondanno1973 [49]; 20 – Bezotosnyj1980 [53]; 21 – Kopatch2025 [14].

pond to the transitions  $2.814(7/2^-) \rightarrow \text{g.s.}(3/2^+)$  in the  $^{39}\text{K}$  nucleus and  $3.736(3^-) \rightarrow \text{g.s.}(0^+)$  in  $^{40}\text{Ca}$ , respectively. Significant  $a_2$  and  $a_4$  coefficients, with no contribution

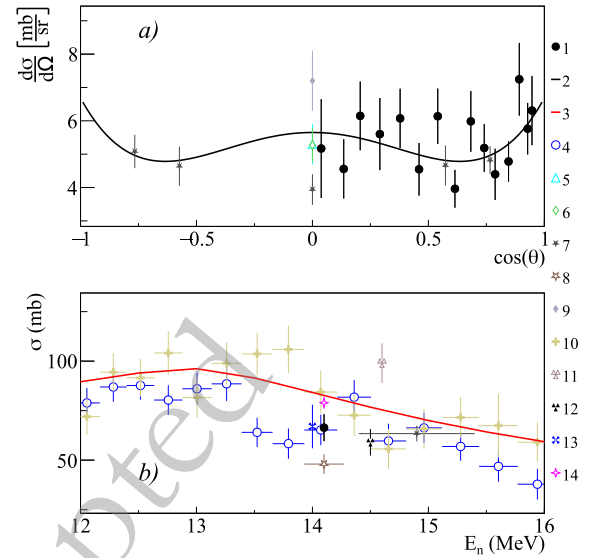


**Fig. 11.** (color online) Differential (a) and total (b) cross-sections of 2.839 MeV  $\gamma$ -ray emission from the  $^{28}\text{Si}(n,n')^{28}\text{Si}$  reactions, compared with experimental data from other authors and theoretical calculations using the TALYS code with default parameters. 1 – present work data; 2 – Legendre polynomial fit of angular distribution from present work; 3 – TALYS calculation; 4 – Negret2013 [57]; 5 – Engesser1967 [19]; 6 – Guoying1992 [54]; 7 – Zhou2011 [56]; 8 – Murata1988 [28]; 9 – Hasegawa1991 [30]; 10 – Boromiza2020 [58]; 11 – Hlavac1999 [42]; 12 – Simakov1998 [85]; 13 – Bezotosnyj1980 [53]; 14 – Kopatch2025 [14].

from  $a_6$ , were observed for the transitions  $0.800(2^-) \rightarrow 0.03(2^-)$  and  $0.892(5^-) \rightarrow \text{g.s.}(4^-)$  in the  $^{40}\text{K}$  nucleus (lines with energies of 0.770 MeV and 0.891 MeV, respectively), as well as for  $3.904(2^+) \rightarrow \text{g.s.}(0^+)$  (the 3.904 MeV line) in the  $^{40}\text{Ca}$  nucleus.

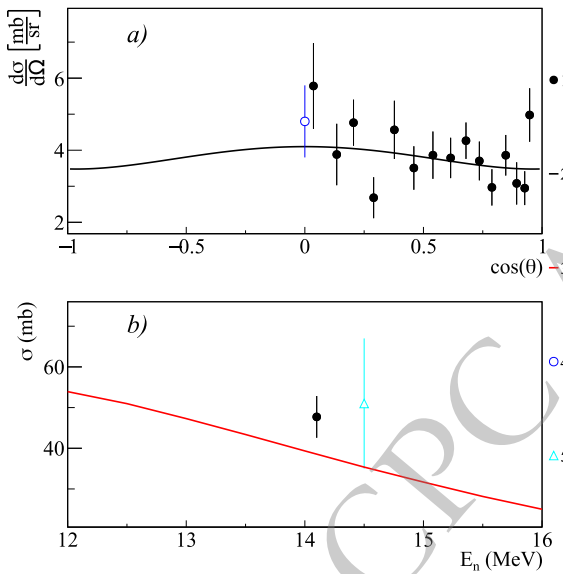
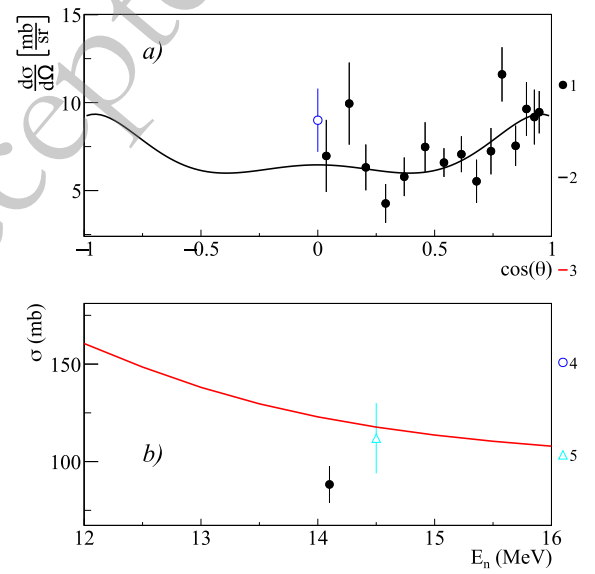
For titanium, in the present work, angular distribu-

**Table 4.** Total emission cross-sections  $\sigma$  and Legendre polynomial expansion coefficients  $a_2$  and  $a_4$  for angular distributions of  $\gamma$ -ray lines emitted during the interaction of 14.1 MeV neutrons with aluminum nuclei. The energies of the initial ( $i$ ) and final ( $f$ ) states are given in MeV.

$E_\gamma$ (MeV)	Reaction	Transition, $E_i (J_i^\pi) \rightarrow E_f (J_f^\pi)$	$\sigma$ (mb)	$a_2$	$a_4$
0.091	$^{27}\text{Al}(n,\alpha)^{24}\text{Na}$	$0.563(2^+) \rightarrow 0.472(1^+)$	$42 \pm 4$	$-0.21 \pm 0.04$	$0.03 \pm 0.06$
0.792	$^{27}\text{Al}(n,n')^{27}\text{Al}$	$3.004(9/2^+) \rightarrow 2.212(7/2^+)$	$26 \pm 3$	$-0.07 \pm 0.07$	$-0.02 \pm 0.10$
0.843	$^{27}\text{Al}(n,n')^{27}\text{Al}$	$0.843(1/2^+) \rightarrow \text{g.s.}(5/2^+)$	$28 \pm 3$	$-0.24 \pm 0.07$	$0.11 \pm 0.10$
0.984	$^{27}\text{Al}(n,p)^{27}\text{Mg}$	$0.984(3/2^+) \rightarrow \text{g.s.}(1/2^+)$	$28 \pm 3$	$0.07 \pm 0.09$	$-0.07 \pm 0.14$
1.014	$^{27}\text{Al}(n,n')^{27}\text{Al}$	$1.014(3/2^+) \rightarrow \text{g.s.}(5/2^+)$	$70 \pm 6$	$0.04 \pm 0.04$	$0.04 \pm 0.06$
1.698	$^{27}\text{Al}(n,p)^{27}\text{Mg}$	$1.698(5/2^+) \rightarrow \text{g.s.}(1/2^+)$	$29 \pm 3$	$0.23 \pm 0.15$	$0.18 \pm 0.20$
1.808	$^{27}\text{Al}(n,d)^{26}\text{Mg}$	$1.808(2^+) \rightarrow \text{g.s.}(0^+)$	$140 \pm 13$	$0.08 \pm 0.01$	$-0.02 \pm 0.02$
2.212	$^{27}\text{Al}(n,n')^{27}\text{Al}$	$2.212(7/2^+) \rightarrow \text{g.s.}(5/2^+)$	$138 \pm 12$	$0.14 \pm 0.02$	$-0.03 \pm 0.02$
2.298	$^{27}\text{Al}(n,n')^{27}\text{Al}$	$4.510(11/2^+) \rightarrow 2.212(7/2^+)$	$29 \pm 3$	$0.34 \pm 0.04$	$-0.03 \pm 0.06$
3.004	$^{27}\text{Al}(n,n')^{27}\text{Al}$	$3.004(9/2^+) \rightarrow \text{g.s.}(5/2^+)$	$108 \pm 11$	$0.20 \pm 0.02$	$0.03 \pm 0.03$

**Table 5.** Total emission cross-sections  $\sigma$  and Legendre polynomial expansion coefficients  $a_2$  and  $a_4$  for angular distributions of  $\gamma$ -ray lines emitted during the interaction of 14.1 MeV neutrons with silicon nuclei. The energies of the initial ( $i$ ) and final ( $f$ ) states are given in MeV.

$E_\gamma$ (MeV)	Reaction	Transition, $E_i(J_i^\pi) \rightarrow E_f(J_f^\pi)$	$\sigma$ (mb)	$a_2$	$a_4$
0.389	$^{28}\text{Si}(n, \alpha)^{25}\text{Mg}$	$0.974(3/2^+) \rightarrow 0.585(1/2^+)$	$32 \pm 5$	$-0.25 \pm 0.25$	$-0.08 \pm 0.35$
0.585	$^{28}\text{Si}(n, \alpha)^{25}\text{Mg}$	$0.585(1/2^+) \rightarrow \text{g.s.}(5/2^+)$	$35 \pm 4$	$0.10 \pm 0.16$	$0.16 \pm 0.21$
1.622	$^{28}\text{Si}(n, p)^{28}\text{Al}$	$1.622(2^+) \rightarrow \text{g.s.}(3^+)$	$43 \pm 5$	$0.01 \pm 0.18$	$-0.27 \pm 0.25$
1.779	$^{28}\text{Si}(n, n')^{28}\text{Si}$ $^{29}\text{Si}(n, 2n)^{28}\text{Si}$	$1.779(2^+) \rightarrow \text{g.s.}(0^+)$	$346 \pm 31$	$0.18 \pm 0.02$	$-0.11 \pm 0.03$
2.271	$^{28}\text{Si}(n, p)^{28}\text{Al}$	$2.271(4^+) \rightarrow \text{g.s.}(3^+)$	$47 \pm 14$	$0.57 \pm 0.70$	$0.54 \pm 0.83$
2.839	$^{28}\text{Si}(n, n')^{28}\text{Si}$	$4.617(4^+) \rightarrow 1.779(2^+)$	$67 \pm 7$	$0.03 \pm 0.10$	$0.23 \pm 0.14$

**Fig. 12.** (color online) Differential (a) and total (b) cross-sections of 0.891 MeV  $\gamma$ -ray emission from the  $^{40}\text{Ca}(n, p)^{40}\text{K}$  reaction, compared with experimental data from other authors and theoretical calculations using the TALYS code with default parameters. 1 – present work data; 2 – Legendre polynomial fit of angular angular distribution from present work; 3 – TALYS calculation; 4 – Engesser1967 [19]; 5 – Simakov1998 [85].**Fig. 13.** (color online) Differential (a) and total (b) cross-sections of 3.736 MeV  $\gamma$ -ray emission from the  $^{40}\text{Ca}(n, n')^{40}\text{Ca}$  reaction, compared with experimental data from other authors and theoretical calculations using the TALYS code with default parameters. 1 – present work data; 2 – Legendre polynomial fit of angular angular distribution from present work; 3 – TALYS calculation; 4 – Engesser1967 [19]; 5 – Simakov1998 [85].

tions and emission cross-sections were obtained for lines with energies of 0.121, 0.130, 0.159, 0.175, 0.370, 0.889, 0.944, 0.983, 1.037, 1.120, 1.312, 1.437, 1.542, 2.375 MeV. It is worth noting that the (n,2n) reaction contributes to all observed  $\gamma$ -transitions excited by inelastic scattering of neutrons on titanium nuclei. As can be seen from Figs. 14 and 15, which present data for the most intense lines with energies of 0.983 and 1.312 MeV in comparison with data from other authors, the total emission cross-sections obtained in the present work agree with most of the data from other authors [53, 60, 62, 63] within the measurement uncertainties, except for data from a recent study [64], which are slightly higher.

The available data on angular distributions for these and other lines are quite fragmentary and represented by only a few measurements [19, 49, 51, 59], of which only two datasets provide more than 1 angular point [19, 49]. Detailed angular distributions for all lines, except 0.983 and 1.312 MeV, were obtained for the first time.

Overall, as can be seen from the approximation results presented in Table 7, for most transitions in titanium nuclei, significant  $a_2$  coefficients were observed in the Legendre polynomial expansion, with negligible contributions from  $a_4$  and  $a_6$  coefficients. An exception is the transition  $0.130(5^+) \rightarrow \text{g.s.}(6^+)$  in the  $^{48}\text{Sc}$  nucleus, for which the angular distribution is nearly isotropic.

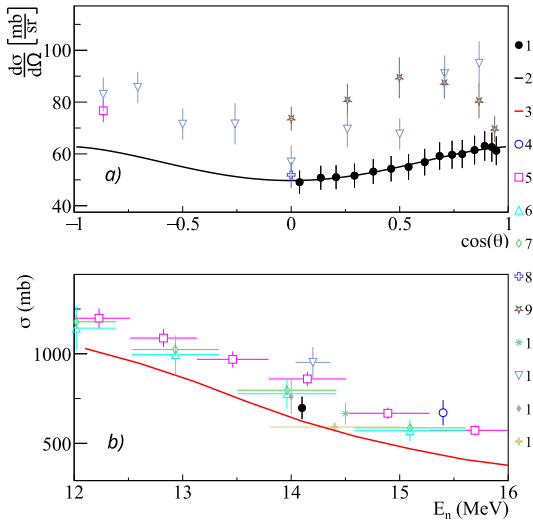


**Fig. 14.** (color online) Differential (a) and total (b) cross-sections of 0.983 MeV  $\gamma$ -ray emission from the  $^{48}\text{Ti}(n,n')^{48}\text{Ti}$  and  $^{49}\text{Ti}(n,2n)^{48}\text{Ti}$  reactions, compared with experimental data from other authors and theoretical calculations using the TALYS code with default parameters. 1 – present work data; 2 – Legendre polynomial fit of angular distribution from present work; 3 – TALYS calculation; 4 – Lashuk1994 [31]; 5 – Olacel2017 [64]; 6 – Arya1967 [59]; 7 – Dashdorj2005 [62]; 8 – Dashdorj2007 [63]; 9 – Engesser1967 [19]; 10 – Connell1975 [51]; 11 – Simakov1998 [85]; 12 – Abbondanno1973 [49]; 13 – Bezotosnyj1980 [53]; 14 – Breunlich1971 [60].

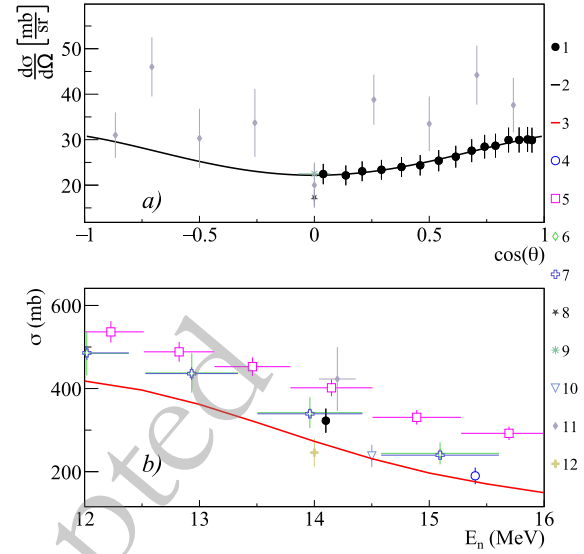


**Fig. 15.** (color online) Differential (a) and total (b) cross-sections of  $\gamma$ -ray emission with energy 1.312 MeV from the reactions  $^{48}\text{Ti}(n,n')^{48}\text{Ti}$  and  $^{49}\text{Ti}(n,2n)^{48}\text{Ti}$ , in comparison with experimental data of other authors and theoretical calculations based on the TALYS program with default parameters. 1 – data from the present work; 2 – angular distribution fit from the present work using Legendre polynomials; 3 – calculation in TALYS; 4 – Lashuk1994 [31]; 5 – Olacel2017 [64]; 6 – Dashdorj2005 [62]; 7 – Dashdorj2007 [63]; 8 – Engesser1967 [19]; 9 – Connell1975 [51]; 10 – Simakov1998 [85]; 11 – Abbondanno1973 [49]; 12 – Bezotosnyj1980 [53].

**Table 6.** Total emission cross sections  $\sigma$  and coefficients of angular distribution expansion in Legendre polynomials  $a_2, a_4$  and  $a_6$  for  $\gamma$ -ray lines emitted in the interaction of 14.1 MeV neutrons with calcium nuclei. The energies of the initial ( $i$ ) and final ( $f$ ) states are given in MeV.

$E_\gamma$ (MeV)	Reaction	Transition, $E_i (J_i^\pi) \rightarrow E_f (J_f^\pi)$	$\sigma$ (mb)	$a_2$	$a_4$	$a_6$
0.770	$^{40}\text{Ca}(n,p)^{40}\text{K}$	$0.800(2^-) \rightarrow 0.030(2^-)$	$40 \pm 5$	$0.10 \pm 0.21$	$0.16 \pm 0.25$	
0.891	$^{40}\text{Ca}(n,p)^{40}\text{K}$	$0.891(5^-) \rightarrow \text{g.s.}(4^-)$	$48 \pm 5$	$-0.13 \pm 0.12$	$0.04 \pm 0.17$	
1.159	$^{40}\text{Ca}(n,p)^{40}\text{K}$	$1.959(2^+) \rightarrow 0.800(2^-)$	$29 \pm 4$	$-0.07 \pm 0.19$		
1.611	$^{40}\text{Ca}(n,\alpha)^{37}\text{Ar}$	$1.611(7/2^-) \rightarrow \text{g.s.}(3/2^+)$	$34 \pm 6$	$0.01 \pm 0.26$	$-0.30 \pm 0.43$	$0.41 \pm 0.47$
2.217	$^{40}\text{Ca}(n,\alpha)^{37}\text{Ar}$	$2.217(7/2^+) \rightarrow \text{g.s.}(3/2^+)$	$21 \pm 3$	$-0.38 \pm 0.20$	$0.11 \pm 0.30$	
2.814	$^{40}\text{Ca}(n,d)^{39}\text{K}$	$2.814(7/2^-) \rightarrow \text{g.s.}(3/2^+)$	$28 \pm 4$	$0.46 \pm 0.23$	$-0.08 \pm 0.25$	$0.49 \pm 0.34$
3.736	$^{40}\text{Ca}(n,n')^{40}\text{Ca}$	$3.736(3^-) \rightarrow \text{g.s.}(0^+)$	$88 \pm 12$	$0.34 \pm 0.15$	$0.12 \pm 0.18$	$-0.15 \pm 0.24$
3.904	$^{40}\text{Ca}(n,n')^{40}\text{Ca}$	$3.904(2^+) \rightarrow \text{g.s.}(0^+)$	$39 \pm 6$	$0.07 \pm 0.22$	$0.26 \pm 0.31$	

#### D. Chromium and Iron

The results of measurements for the most intense  $\gamma$ -ray lines emitted during the interaction of 14.1 MeV neutrons with chromium and iron nuclei are presented in Figs. 16–19 and Table 8 and 9.

For chromium, a relatively large amount of experimental data is available for both angular distributions and total emission cross sections. In this work, emission cross

sections and angular distributions were obtained for  $\gamma$ -ray lines with energies of 0.647, 0.704, 0.744, 0.935, 1.333, 1.434, and 1.530 MeV emitted in the reactions  $^{52}\text{Cr}(n,n')^{52}\text{Cr}$  and  $^{53}\text{Cr}(n,2n)^{52}\text{Cr}$ . It is worth noting that the  $(n,2n)$  reaction contributes to all observed  $\gamma$ -transitions excited by inelastic scattering of neutrons on chromium nuclei.

For the most intense lines with energies of 0.935 and 1.434 MeV (see Figs. 16 and 17), agreement is observed

**Table 7.** Total emission cross sections  $\sigma$  and coefficients of angular distribution expansion in Legendre polynomials  $a_2$  and  $a_4$  for  $\gamma$ -ray lines emitted in the interaction of 14.1 MeV neutrons with titanium nuclei. The energies of the initial ( $i$ ) and final ( $f$ ) states are given in MeV.

$E_\gamma$ (MeV)	Reaction	Transition, $E_i (J_i^\pi) \rightarrow E_f (J_f^\pi)$	$\sigma$ (mb)	$a_2$	$a_4$
0.121	$^{48}\text{Ti}(n, p)^{48}\text{Sc}$	$0.252(4^+) \rightarrow 0.130(5^+)$	$51 \pm 8$	$0.39 \pm 0.31$	$-0.03 \pm 0.46$
0.130	$^{48}\text{Ti}(n, p)^{48}\text{Sc}$	$0.130(5^+) \rightarrow \text{g.s.}(6^+)$	$47 \pm 5$	$0.01 \pm 0.09$	$-0.22 \pm 0.13$
0.159	$^{47}\text{Ti}(n, n')^{47}\text{Ti}$ $^{48}\text{Ti}(n, 2n)^{47}\text{Ti}$	$0.159(7/2^-) \rightarrow \text{g.s.}(5/2^-)$	$187 \pm 17$	$-0.27 \pm 0.01$	$-0.03 \pm 0.02$
0.175	$^{48}\text{Ti}(n, n')^{48}\text{Ti}$ $^{49}\text{Ti}(n, 2n)^{48}\text{Ti}$	$3.508(6^+) \rightarrow 3.333(6^+)$	$43 \pm 4$	$0.42 \pm 0.05$	$-0.12 \pm 0.07$
0.370	$^{48}\text{Ti}(n, p)^{48}\text{Sc}$	$0.622(3^+) \rightarrow 0.252(4^+)$	$26 \pm 3$	$0.15 \pm 0.08$	$-0.07 \pm 0.11$
0.889	$^{46}\text{Ti}(n, n')^{46}\text{Ti}$ $^{47}\text{Ti}(n, 2n)^{46}\text{Ti}$	$0.889(2^+) \rightarrow \text{g.s.}(0^+)$	$523 \pm 48$	$0.12 \pm 0.03$	$0.01 \pm 0.04$
0.944	$^{48}\text{Ti}(n, n')^{48}\text{Ti}$ $^{49}\text{Ti}(n, 2n)^{48}\text{Ti}$	$3.239(4^+) \rightarrow 2.295(4^+)$	$65 \pm 6$	$0.24 \pm 0.04$	$0.12 \pm 0.06$
0.983	$^{48}\text{Ti}(n, n')^{48}\text{Ti}$ $^{49}\text{Ti}(n, 2n)^{48}\text{Ti}$	$0.983(2^+) \rightarrow \text{g.s.}(0^+)$	$700 \pm 63$	$0.16 \pm 0.01$	$-0.04 \pm 0.01$
1.037	$^{48}\text{Ti}(n, n')^{48}\text{Ti}$ $^{49}\text{Ti}(n, 2n)^{48}\text{Ti}$	$3.333(6^+) \rightarrow 2.295(4^+)$	$72 \pm 7$	$0.42 \pm 0.04$	$-0.01 \pm 0.06$
1.120	$^{46}\text{Ti}(n, n')^{46}\text{Ti}$ $^{47}\text{Ti}(n, 2n)^{46}\text{Ti}$	$2.009(4^+) \rightarrow 0.889(2^+)$	$200 \pm 19$	$0.29 \pm 0.05$	$-0.04 \pm 0.06$
1.312	$^{48}\text{Ti}(n, n')^{48}\text{Ti}$ $^{49}\text{Ti}(n, 2n)^{48}\text{Ti}$	$2.295(4^+) \rightarrow 0.983(2^+)$	$323 \pm 29$	$0.24 \pm 0.01$	$-0.04 \pm 0.01$
1.438	$^{48}\text{Ti}(n, n')^{48}\text{Ti}$ $^{49}\text{Ti}(n, 2n)^{48}\text{Ti}$	$2.421(2^+) \rightarrow 0.983(2^+)$	$59 \pm 6$	$0.15 \pm 0.06$	$-0.01 \pm 0.08$
1.542	$^{49}\text{Ti}(n, n')^{49}\text{Ti}$ $^{49}\text{Ti}(n, 2n)^{50}\text{Ti}$	$1.542(11/2^-) \rightarrow \text{g.s.}(7/2^-)$	$659 \pm 61$	$0.21 \pm 0.05$	$0.08 \pm 0.06$
2.240	$^{48}\text{Ti}(n, n')^{48}\text{Ti}$ $^{49}\text{Ti}(n, 2n)^{48}\text{Ti}$	$3.224(3^+) \rightarrow 0.983(2^+)$	$36 \pm 3$	$0.15 \pm 0.05$	$-0.22 \pm 0.09$
2.375	$^{48}\text{Ti}(n, n')^{48}\text{Ti}$ $^{49}\text{Ti}(n, 2n)^{48}\text{Ti}$	$3.358(3^-) \rightarrow 0.983(2^+)$	$89 \pm 8$	$-0.12 \pm 0.02$	
2.633	$^{48}\text{Ti}(n, n')^{48}\text{Ti}$ $^{49}\text{Ti}(n, 2n)^{48}\text{Ti}$	$3.617(3^+) \rightarrow 0.983(2^+)$	$21 \pm 2$	$-0.19 \pm 0.13$	$-0.01 \pm 0.18$

between the results of this work and data from other authors [49, 50, 59, 60, 65–69], both in angular distributions and total emission cross sections.

It should be noted that all measured angular distributions exhibit a pronounced  $a_2$  coefficient in the Legendre polynomial expansion (see Table 8), while the influence of the  $a_4$  coefficient is negligible.

Data obtained for iron in the present work include angular distributions and total emission cross sections for  $\gamma$ -ray lines with energies of 0.125, 0.212, 0.846, 0.931, 1.037, 1.238, 1.303, 1.408, 1.670, 1.810, and 2.598 MeV, generated in  $(n, p)$ ,  $(n, d)$ ,  $(n, n')$ , and  $(n, 2n)$  reactions on iron isotopes. It is worth noting that the  $(n, 2n)$  reaction

contributes to all observed  $\gamma$ -transitions excited by inelastic scattering of neutrons on iron nuclei.

Comparison of experimental data obtained in the present work with data from other authors [19, 24, 26, 30, 31, 47–49, 52, 55, 59, 60, 65, 67, 70, 72–77, 79–84] for the most intense lines (0.846 and 1.238 MeV) is shown in Figs. 18 and 19. As can be seen from the figures, there is a considerable amount of experimental data available for these lines, both for angular distributions and total cross sections. The values of both total and differential cross sections obtained in this work for these lines agree with data from other authors within the existing scatter of data points.

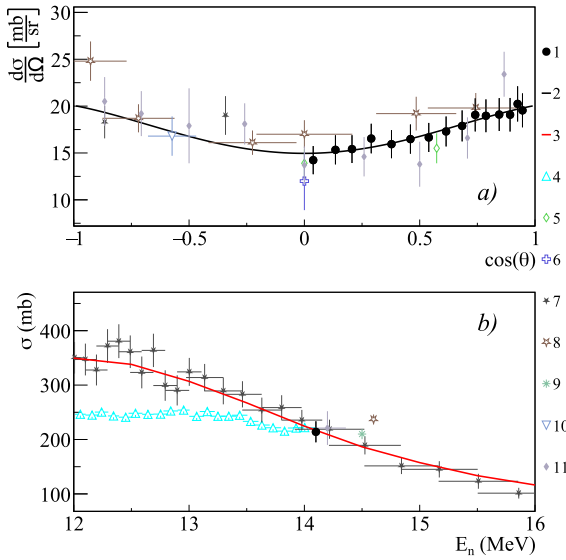


**Fig. 16.** Differential (a) and total (b) cross sections of  $\gamma$ -ray emission with energy 0.935 MeV from the reactions  $^{52}\text{Cr}(n,n')^{52}\text{Cr}$  and  $^{53}\text{Cr}(n,2n)^{52}\text{Cr}$ , in comparison with experimental data of other authors and theoretical calculations based on the TALYS program with default parameters. 1 – data from the present work; 2 – angular distribution fit from the present work using Legendre polynomials; 3 – calculation in TALYS; 4 – Voss1975 [66]; 5 – Clayeux1969 [20]; 6 – Kinney1972 [65]; 7 – Mihailescu2007 [69]; 8 – Oblozinsky1992 [68]; 9 – Simakov1998 [85]; 10 – Yamamoto1978 [67]; 11 – Abbondanno1973 [49].

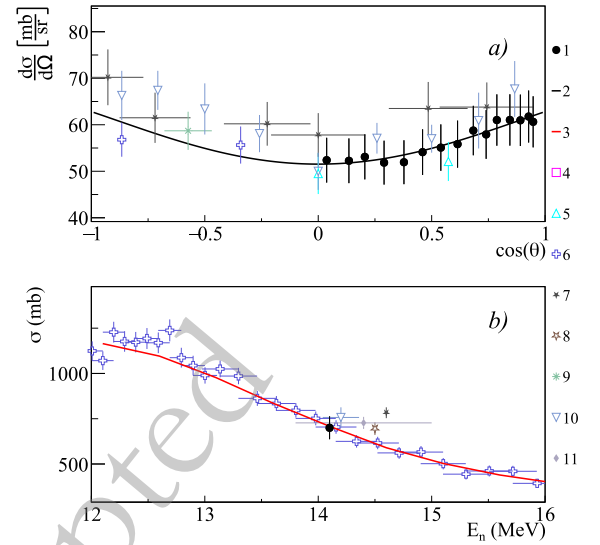


**Fig. 17.** Differential (a) and total (b) cross sections of  $\gamma$ -ray emission with energy 1.434 MeV from the reactions  $^{52}\text{Cr}(n,n')^{52}\text{Cr}$  and  $^{53}\text{Cr}(n,2n)^{52}\text{Cr}$ , in comparison with experimental data of other authors and theoretical calculations based on the TALYS program with default parameters. 1 – data from the present work; 2 – angular distribution fit from the present work using Legendre polynomials; 3 – calculation in TALYS; 4 – Voss1975 [66]; 5 – Clayeux1969 [20]; 6 – Mihailescu2007 [69]; 7 – Oblozinsky1992 [68]; 8 – Simakov1998 [85]; 9 – Yamamoto1978 [67]; 10 – Abbondanno1973 [49]; 11 – Breunlich1971 [60].

**Table 8.** Total emission cross sections  $\sigma$  and coefficients of angular distribution expansion in Legendre polynomials  $a_2$  and  $a_4$  for  $\gamma$ -ray lines emitted in the interaction of 14.1 MeV neutrons with chromium nuclei. The energies of the initial ( $i$ ) and final ( $f$ ) states are given in MeV.

$E_\gamma$ (MeV)	Reaction	Transition, $E_i (J_i^\pi) \rightarrow E_f (J_f^\pi)$	$\sigma$ (mb)	$a_2$	$a_4$
0.647	$^{52}\text{Cr}(n,n')^{52}\text{Cr}$	3.415( $4^+$ ) $\rightarrow$ 2.767( $4^+$ )	$52 \pm 5$	$0.25 \pm 0.06$	$-0.02 \pm 0.08$
	$^{53}\text{Cr}(n,2n)^{52}\text{Cr}$				
0.744	$^{52}\text{Cr}(n,n')^{52}\text{Cr}$	3.113( $6^+$ ) $\rightarrow$ 2.369( $4^+$ )	$52 \pm 5$	$0.39 \pm 0.11$	$-0.21 \pm 0.15$
	$^{53}\text{Cr}(n,2n)^{52}\text{Cr}$				
0.935	$^{52}\text{Cr}(n,n')^{52}\text{Cr}$	2.369( $4^+$ ) $\rightarrow$ 1.434( $2^+$ )	$214 \pm 19$	$0.22 \pm 0.02$	$-0.04 \pm 0.02$
	$^{53}\text{Cr}(n,2n)^{52}\text{Cr}$				
1.333	$^{52}\text{Cr}(n,n')^{52}\text{Cr}$	2.767( $4^+$ ) $\rightarrow$ 1.434( $2^+$ )	$162 \pm 15$	$0.19 \pm 0.01$	$-0.05 \pm 0.02$
	$^{53}\text{Cr}(n,2n)^{52}\text{Cr}$				
1.434	$^{52}\text{Cr}(n,n')^{52}\text{Cr}$	1.434( $2^+$ ) $\rightarrow$ g.s.( $0^+$ )	$700 \pm 63$	$0.14 \pm 0.01$	$-0.01 \pm 0.02$
	$^{53}\text{Cr}(n,2n)^{52}\text{Cr}$				
1.530	$^{52}\text{Cr}(n,n')^{52}\text{Cr}$	2.964( $2^+$ ) $\rightarrow$ 1.434( $2^+$ )	$40 \pm 4$	$-0.08 \pm 0.07$	$-0.03 \pm 0.10$
	$^{53}\text{Cr}(n,2n)^{52}\text{Cr}$				

From the Legendre polynomial expansion coefficients presented in Table 9, it is evident that for all transitions – except for the  $2.657(2^+) \rightarrow 0.846(2^+)$  transition in  $^{56}\text{Fe}$  (1.810 MeV line) and the  $0.125(7/2^-) \rightarrow \text{g.s.}(5/2^-)$

transition in  $^{55}\text{Mn}$  (0.125 MeV line) – there is a significant contribution from the  $a_2$  coefficient, with a minor or negligible contribution from the  $a_4$  coefficient.

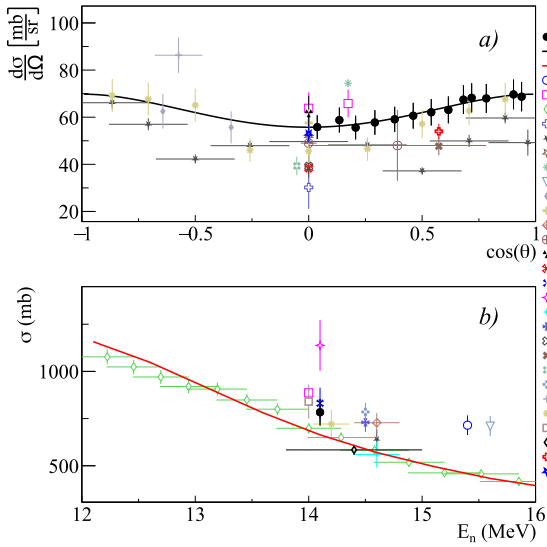


**Fig. 18.** (color online) Differential (a) and total (b) cross sections of  $\gamma$ -ray emission with energy 0.846 MeV from the reactions  $^{56}\text{Fe}(n,n')^{56}\text{Fe}$  and  $^{57}\text{Fe}(n,2n)^{56}\text{Fe}$ , in comparison with experimental data of other authors and theoretical calculations based on the TALYS program with default parameters. 1 – data from the present work; 2 – angular distribution fit from the present work using Legendre polynomials; 3 – calculation in TALYS; 4 – Lashuk1994 [31]; 5 – Shalabi1983 [75]; 6 – Negret2014 [79]; 7 – Arya1967 [59]; 8 – Degtyarev1977 [73]; 9 – Sukhanov1970 [72]; 10 – Joensson1969 [71]; 11 – Broder1970 [80]; 12 – Drake1978 [52]; 13 – Engesser1967 [19]; 14 – Western1965 [81]; 15 – Prud'homme1960 [47]; 16 – Hasegawa1991 [30]; 17 – Drosz2002 [55]; 18 – Mitsuda2002 [82]; 19 – Bostrom1959 [70]; 20 – Martin1965 [48]; 21 – Antalik1980 [83]; 22 – Nelson2005 [84]; 23 – Hlavac1983 [76]; 24 – Xiamin1982 [74]; 25 – Zong1979 [26]; 26 – Simakov1998 [85]; 27 – Yamamoto1978 [67]; 28 – Abbondanno1973 [49]; 29 – Bezotosnyi1975 [24]; 30 – Breunlich1971 [60]; 31 – Jinqiang1988 [77]; 32 – Hongyu1986 [46].

## V. CONCLUSION

In this work, differential cross-sections of  $\gamma$ - emission generated in reactions under the action of 14.1 MeV neutrons on the nuclei of carbon, aluminum, silicon, calcium, chromium and iron were measured. The measurements were performed using four  $\text{LaBr}_3(\text{Ce})$  scintillation detectors positioned at angles of  $25^\circ$ ,  $45^\circ$ ,  $60^\circ$ , and  $70^\circ$  relative to the axis of the generator target – the center of the sample. A key feature of this study was the implementation of the tagged neutron method. The experiments utilized a neutron generator capable of producing 16 separate tagged neutron beams. Combined with the detector system, this enabled measurements of differential cross sections at 64 discrete angles in the  $17^\circ$ – $89^\circ$  range. Corrections for multiple neutron scattering and attenu-

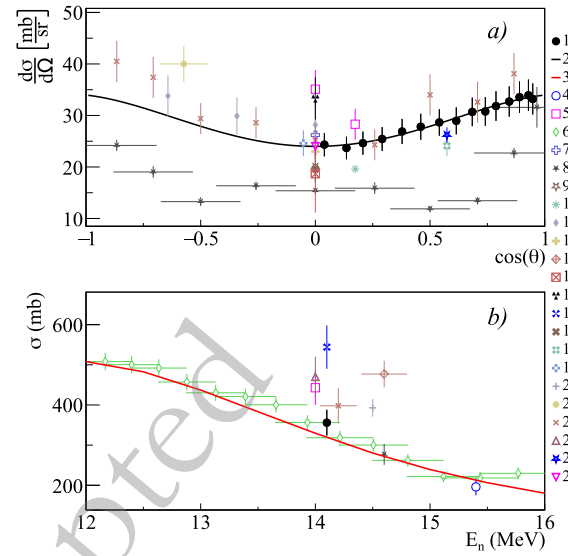


**Fig. 19.** (color online) Differential (a) and total (b) cross sections of  $\gamma$ -ray emission with energy 1.238 MeV from the reactions  $^{56}\text{Fe}(n,n')^{56}\text{Fe}$  and  $^{57}\text{Fe}(n,2n)^{56}\text{Fe}$ , in comparison with experimental data of other authors and theoretical calculations based on the TALYS program with default parameters. 1 – data from the present work; 2 – angular distribution fit from the present work using Legendre polynomials; 3 – calculation in TALYS; 4 – Lashuk1994 [31]; 5 – Shalabi1983 [75]; 6 – Negret2014 [79]; 7 – Arya1967 [59]; 8 – Degtyarev1977 [73]; 9 – Sukhanov1970 [72]; 10 – Joensson1969 [71]; 11 – Drake1978 [52]; 12 – Engesser1967 [19]; 13 – Western1965 [81]; 14 – Kinney1972 [65]; 15 – Hasegawa1991 [30]; 16 – Mitsuda2002 [82]; 17 – Hlavac1983 [76]; 18 – Xiamin1982 [74]; 19 – Zong1979 [26]; 20 – Simakov1998 [85]; 21 – Yamamoto1978 [67]; 22 – Abbondanno1973 [49]; 23 – Bezotosnyi1975 [24]; 24 – Jinqiang1988 [77]; 25 – Hongyu1986 [46].

ation,  $\gamma$ -ray attenuation, and total detection efficiency – calculated using GEANT4 – were systematically applied. Verification measurements were conducted to validate these correction factors. The analysis yielded angular distribution data for the 4.439 MeV  $\gamma$ -line from carbon, 10  $\gamma$ -lines from aluminum reactions, 6  $\gamma$ -lines from silicon reactions, 8  $\gamma$ -lines from calcium reactions, 16  $\gamma$ -lines from titanium reactions, 6  $\gamma$ -lines from chromium reactions, and 14  $\gamma$ -lines from iron reactions. All angular distributions were approximated through expansion in even-order Legendre polynomials, followed by full solid-angle integration to determine total emission cross sections. The total systematic uncertainty of the obtained data was estimated to be 9.1%.

## ACKNOWLEDGEMENTS

*We thank D. N. Borisov and S. I. Negovetov for their help in preparing the experiments.*

**Table 9.** Total emission cross sections  $\sigma$  and coefficients of angular distribution expansion in Legendre polynomials  $a_2$  and  $a_4$  for  $\gamma$ -ray lines emitted in the interaction of 14.1 MeV neutrons with iron nuclei. The energies of the initial ( $i$ ) and final ( $f$ ) states are given in MeV.

$E_\gamma$ (MeV)	Reaction	Transition, $E_i (J_i^\pi) \rightarrow E_f (J_f^\pi)$	$\sigma$ (mb)	$a_2$	$a_4$
0.125	$^{56}\text{Fe}(n, d)^{55}\text{Mn}$	$0.125(7/2^-) \rightarrow \text{g.s.}(5/2^-)$	$46 \pm 4$	$-0.11 \pm 0.04$	$-0.19 \pm 0.06$
0.212	$^{56}\text{Fe}(n, p)^{56}\text{Mn}$	$0.212(4^+) \rightarrow \text{g.s.}(3^+)$	$39 \pm 4$	$-0.18 \pm 0.09$	$0.07 \pm 0.12$
	$^{57}\text{Fe}(n, d)^{56}\text{Mn}$				
0.367	$^{56}\text{Fe}(n, n')^{56}\text{Fe}$	$3.756(6^+) \rightarrow 3.389(6^+)$	$10 \pm 3$	$0.16 \pm 0.60$	$0.15 \pm 0.74$
	$^{57}\text{Fe}(n, 2n)^{56}\text{Fe}$				
0.411	$^{54}\text{Fe}(n, n')^{54}\text{Fe}$	$2.949(6^+) \rightarrow 2.538(4^+)$	$20 \pm 2$	$-0.07 \pm 0.04$	$0.02 \pm 0.05$
	$^{56}\text{Fe}(n, 2n)^{55}\text{Fe}$	$0.411(1/2^-) \rightarrow \text{g.s.}(3/2^-)$			
0.477	$^{56}\text{Fe}(n, 2n)^{55}\text{Fe}$	$1.408(7/2^-) \rightarrow 0.931(5/2^-)$	$17 \pm 3$	$-0.28 \pm 0.27$	$0.05 \pm 0.36$
0.846	$^{56}\text{Fe}(n, n')^{56}\text{Fe}$	$0.856(2^+) \rightarrow \text{g.s.}(0^+)$	$784 \pm 71$	$0.17 \pm 0.01$	$-0.05 \pm 0.02$
	$^{57}\text{Fe}(n, 2n)^{56}\text{Fe}$				
0.931	$^{56}\text{Fe}(n, 2n)^{55}\text{Fe}$	$0.931(5/2^-) \rightarrow \text{g.s.}(3/2^-)$	$78 \pm 7$	$0.20 \pm 0.02$	$-0.03 \pm 0.03$
1.038	$^{56}\text{Fe}(n, n')^{56}\text{Fe}$	$3.122(4^+) \rightarrow 2.085(4^+)$	$72 \pm 7$	$0.24 \pm 0.04$	$-0.01 \pm 0.06$
	$^{57}\text{Fe}(n, 2n)^{56}\text{Fe}$				
1.238	$^{56}\text{Fe}(n, n')^{56}\text{Fe}$	$2.085(4^+) \rightarrow 0.846(2^+)$	$356 \pm 32$	$0.26 \pm 0.01$	$-0.06 \pm 0.01$
	$^{57}\text{Fe}(n, 2n)^{56}\text{Fe}$				
1.303	$^{56}\text{Fe}(n, n')^{56}\text{Fe}$	$3.388(6^+) \rightarrow 2.085(4^+)$	$136 \pm 12$	$0.31 \pm 0.02$	$-0.09 \pm 0.03$
	$^{57}\text{Fe}(n, 2n)^{56}\text{Fe}$				
1.408	$^{54}\text{Fe}(n, n')^{54}\text{Fe}$	$1.408(2^+) \rightarrow \text{g.s.}(0^+)$	$33 \pm 3$	$0.17 \pm 0.04$	$-0.08 \pm 0.05$
	$^{56}\text{Fe}(n, 2n)^{55}\text{Fe}$	$1.408(7/2^-) \rightarrow \text{g.s.}(3/2^-)$			
1.670	$^{56}\text{Fe}(n, n')^{56}\text{Fe}$	$3.755(6^+) \rightarrow 2.085(4^+)$	$43 \pm 4$	$0.42 \pm 0.04$	$-0.15 \pm 0.05$
	$^{57}\text{Fe}(n, 2n)^{56}\text{Fe}$				
1.810	$^{56}\text{Fe}(n, n')^{56}\text{Fe}$	$2.657(2^+) \rightarrow 0.846(2^+)$	$51 \pm 5$	$0.02 \pm 0.07$	$-0.12 \pm 0.11$
	$^{57}\text{Fe}(n, 2n)^{56}\text{Fe}$				
2.598	$^{56}\text{Fe}(n, n')^{56}\text{Fe}$	$3.445(3^+) \rightarrow 0.846(2^+)$	$31 \pm 3$	$-0.31 \pm 0.03$	$-0.06 \pm 0.04$
	$^{57}\text{Fe}(n, 2n)^{56}\text{Fe}$				

## References

- [1] Karolina Kolos, Vladimir Sobes, Ramona Vogt, *et al.*, *Phys. Rev. Research* **4**, 021001 (2022)
- [2] I. Ruskov, Yu. Kopatch, V. Bystritsky, *et al.*, *EPJ Web Conf.* **146**, 03024 (2017)
- [3] I. Ruskov, Yu. Kopach, V. Bystritsky, *et al.*, *EPJ Web Conf.* **256**, 00014 (2021)
- [4] Vladivoj Valkovic, in *14 MeV Neutrons: Physics and Application*, Vol. 2., edited by Vladivoj Valkovic (Boca Raton: CRC Press, 2016), p. 17; <https://doi.org/10.1201/b18837>
- [5] Vladivoj Valkovic, in *14 MeV Neutrons: Physics and Application*, Vol. 7., edited by Vladivoj Valkovic (Boca Raton: CRC Press, 2016), p. 256; <https://doi.org/10.1201/b18837>
- [6] Ilya Bolshakov, Maxim Kolesnik, Maxim Sorokin, *et al.*, *Int. J. Miner. Process. Extr. Metall.* **5**(4), 54 (2020)
- [7] V.Y. Alexakhin, A.I. Akhunova, E.A. Razinkov, *et al.*, *Phys. Atom. Nuclei* **85**, 1866 (2022)
- [8] Bishnoi, S., Patel, T., Thomas, R. G., *et al.*, *Eur. Phys. J. Plus* **135**, 428 (2020)
- [9] D.N. Grozdanov, N.A. Fedorov, V.M. Bystritski, *et al.*, *Phys. Atom. Nuclei* **81**, 588 (2018)
- [10] N.A. Fedorov, T.Y. Tretyakova, V.M. Bystritsky, *et al.*, *Phys. Atom. Nuclei* **82**, 343 (2019)
- [11] N.A. Fedorov, D.N. Grozdanov, Y.N. Kopatch, *et al.*, *Eur. Phys. J. A* **57**, 194 (2021)
- [12] I.D. Dashkov, N.A. Fedorov, D.N. Grozdanov, *et al.*, *Bull. Russ. Acad. Sci. Phys.* **86**, 893 (2022)
- [13] Kopach, Y. N., Sapozhnikov, M. G., *Phys. Part. Nuclei* **55**, 55 (2024)
- [14] Kopatch, Y. N., Grozdanov, D. N., Fedorov, N. A., *et al.*, *Phys. Part. Nuclei Lett.* **22**, 276 (2025)
- [15] V. E. Scherrer, R. B. Theus, W. R. Faust, *Phys. Rev.* **91**,

- 1476 (1953)
- [16] J. Benveniste, A.C. Mitchell, C.D. Schrader, *et al.*, *Nucl. Phys.* **19**, 448 (1960)
- [17] D.T. Stewart, P.W. Martin, *Nucl. Phys.* **60**(2), 349 (1964)
- [18] I.L. Morgan, J.B. Ashe, D.O. Nellis, Div. of Tech. Info. U.S. AEC Reports, No. 22012, (Texas Nuclear Corp., Austin, TX, USA, 1964), p.158; EXFOR data: <https://www-nds.iaea.org/EXFOR/12695>
- [19] F. C. Engesser and W. E. Thompson, *J. Nucl. Energy* **21**(6), 487 (1967)
- [20] G. Clayeux, G. Grenier, Saclay Reports, No.3807, (Centre d'Etudes de Limeil, Villeneuve-Saint-Georges, France, Centre d'Etudes Nucleaires, 1969).
- [21] T.C. Martin, G.H. Williams, Oak Ridge Operations Office, contract report, No. 2791-32, (Texas Nuclear Corp., Austin, TX, USA, 1971), p.7
- [22] D. Spaargaren, C.C. Jonker, *Nucl. Phys. A* **161**(2), 354 (1971)
- [23] V.C. Rogers, V.J. Orphan, C.G. Hoot, *et al.*, *Nucl. Sci. Eng.* **58**(3), 298 (1975)
- [24] V. M. Bezotosnyi, V. M. Gorbachev, L. M. Suvorov, *et al.*, *Yad. Konst.* **19**, 7 (1975)
- [25] J.K. Dickens, G.L. Morgan, G.T. Chapman, *et al.*, *Nucl. Sci. Eng.* **62**, 515 (1977)
- [26] S. Zong-Ren, *et al.*, *Chin. J. of Nucl. Phys.* **1**, 45 (1979)
- [27] Y. Hino, S. Itagaki, T. Yamamoto, *et al.*, Dept. of Nucl. Engineering Reports, No. 34, (Tohoku Univ., Sendai, Japan, 1979).
- [28] I. Murata, J. Yamamoto, A. Takahashi, Differential cross sections for gamma-ray production by 14 MeV neutrons with several elements in structural materials, in *Proceedings of the International Conference on Nuclear Data for Science and Technology held at Mito, Japan, May 30-June 3*, edited by S.Igarasi, (Japan: Japan Atomic Energy Research Institute, 1988), p.275; <https://www.ndc.jaea.go.jp/nd1988/>
- [29] Zhou Hongyu, Yan Yiming, Tanglin, Wen Shenlin, *et al.*, *Chinese J. of Nuclear Physics* **11**(2), 63 (1989)
- [30] K. Hasegawa, M. Mizumoto, S. Chiba, *et al.*, Gamma-ray production cross section measurements of some structural materials between 7.8 and 13.0 MeV, in *Proceedings of the International Conference on Nuclear Data for Science and Technology, held at the Forschungszentrum Julich, Fed. Rep. of Germany, 13-17 May 1991*, edited by Syed M. Qaim, (Germany: Springer-Verlag Berlin Heidelberg, 1992), p. 329; <https://doi.org/10.1007/978-3-642-58113-7>
- [31] A.I. Lashuk, I.P. Sadokhin, *Vop. At. Nauki i Tekhn.*, Ser.Yaderno-Reak. Konstanty **1**, 26 (1994)
- [32] I.M. Kadenko, V.A. Plujko, B.M. Bondar, *et al.*, *Yaderna Fizika ta Energetika* **17**, 349 (2016)
- [33] A. M. McEvoy, H. W. Herrmann, Y. Kim, *et al.*, *Phys. Rev. C* **103**, 064607 (2021)
- [34] K. J. Kelly, M. Devlin, J. M. O'Donnell, *et al.*, *Phys. Rev. C* **104**, 064614 (2021)
- [35] K. J. Kelly, M. Devlin, J. M. O'Donnell, *et al.*, *Phys. Rev. C* **108**, 014603 (2023)
- [36] J. M. Gordon, B. L. Goldblum, J. A. Brown, *et al.*, *Phys. Rev. C* **111**, 044608 (2025)
- [37] G.L.Morgan, T.A.Love, J.K.Dickens, *et al.*, *Nucl. Sci. Engineering* **62**, 515 (1977)
- [38] Grozdanov, D. N., Prusachenko, P. S., Fedorov, *Eur. Phys. J. A* **61**, 224 (2025)
- [39] E.M.Burymov, *Sov. J. Nucl. Phys.* **9**, 546 (1969)
- [40] V.N. Bochkarev, V.V. Nefedov, *Sov. J. Nucl. Phys.* **1**, 574 (1965)
- [41] A. Pavlik, H. Hitzenberger-Schauer, H. Vonach, *et al.*, *Phys. Rev. C* **57**, 2416 (1998)
- [42] S. Hlavac, M. Benovic, E. Betak, *et al.*, Cross Sections for Discrete  $\gamma$  Ray Production in Interactions of 14.6 MeV Neutrons with Light and Medium Heavy Nuclei, IAEA Nucl. Data Section report to the I.N.D.C., Rep. No.412, p.12 (1999), (IAEA, Vienna, Austria, 1999); <http://www-nds.iaea.org/publications/indc/indc-nds-0412/>
- [43] V. C. Rogers, V. J. Orphan, C. G. Hoot, *et al.*, Spectral gamma-ray production cross-section measurements from threshold to 20 MeV, in *Proceedings of the Conference on Nuclear Cross Sections and Technology, Washington, USA, 1975*, edited by Roald A. Schrack, Charles D. Bowman, (USA: Department of Commerce, National Bureau of Standards, Institute for Basic Standards, Center for Radiation Research, 1975), Vol.2, p.766; <https://nvlpubs.nist.gov/nistpubs/Legacy/SP/nbsspecialpublication425v2.pdf>
- [44] H. Zhou, G. Huang, *Nucl. Sci. Eng.* **125**(1), 61 (1997)
- [45] K. Nyberg-Ponnert, B. Jonsson, and I. Bergqvist, *Phys. Scr.* **4**, 165 (1971)
- [46] Z. Hongyu, T. Lin, Y. Yiming, *et al.*, Gamma ray production cross sections for the interactions of 14.9 MeV neutrons with C, Al, V, Fe and Nb at 90 degrees, Chinese report to the I.N.D.C., Rep. No INDC(CPR)-010/L, (IAEA NDC, Vienna, Austria, 1986); <https://www-nds.iaea.org/publications/indc/indccpr010L.pdf>
- [47] J. T. Prud'homme, I. L. Morgan, J. H. MC. Crary *et al.*, A study of neutrons and gamma rays from neutron induced reactions in several elements, Air Force Spec. Weap. Center Kirtland A.F.B. Repts., Rep. No 60-30, (Texas Nuclear Corp., Austin, Texas, USA, 1960).
- [48] P.W. Martin, D.T. Stewart, *J. Nucl. Energy* **19**(6), 447 (1965)
- [49] U. Abbondanno, R. Giacomich, M. Lagonegro, *et al.*, *J. Nucl. Energy* **27**(4), 4 (1973)
- [50] G. Grenier, B. Duchemin, D. Parisot, Differential gamma-ray production cross sections measured in Si( $n,X\gamma$ ), Cr( $n,X\gamma$ ) and Ni( $n,X\gamma$ ) reactions for incident neutrons between 3 and 7 MeV and also at 14.1 MeV (in French), Report from CEC-Countries and CEC to NEANDC, Rep. No. 161U, (CEA/DAM Ile-de-France, Bruyeres-le-Chatel, Arpajon, France, 1974); <https://inis.iaea.org/records/jwywez06>
- [51] K.A. Connell, A.J. Cox, *Int. J. Appl. Radiat. Isot.* **26**(2), 71 (1975)
- [52] D. M. Drake, E. D. Arthur, M. G. Silbert, *Nucl. Sci. Eng.* **65**(1), 1 (1978)
- [53] V.M. Bezotosnyj, V.M.Gorbachjov, M.S.Shvetsov, *et al.*, The spectra and formation cross-sections of the discrete gamma-lines in the nonelastic interaction of 14 MeV neutrons with Mg, Si, P, S, Ti and Zn nuclei (In Russian), USSR report to the I.N.D.C., Rep. No. INDC(CCP)-169 VOL IV, (IAEA NDS, Vienna, Austria, 1980), p.21; [https://www-nds.iaea.org/publications/indc/indc-ccp-169\\_vol\\_II.pdf](https://www-nds.iaea.org/publications/indc/indc-ccp-169_vol_II.pdf)
- [54] Guoying Fan, Hongyu Zhou, Xiaoge Zhu, *et al.*, Progress in the Measurement of Gamma-Ray Production Cross Sections Induced by 14.9 MeV Neutrons, In: Qaim, S.M. (eds) In *Proceedings of the International Conference on Nuclear Data for Science and Technology held at the*

- Forschungszentrum Jülich, Fed. Rep. of Germany, 13-17 May 1991, edited by Syed M. Qaim, (Germany: Springer-Verlag Berlin Heidelberg, 1992), p. 332; [https://doi.org/10.1007/978-3-642-58113-7\\_95](https://doi.org/10.1007/978-3-642-58113-7_95)
- [55] M. Drosig, R. C. Haight, D. M. Drake, Double-differential gamma-ray production: cross sections and spectra of Al, Si and Fe for 8.51, 10.00, 12.24 and 14.24 MeV neutrons, Los Alamos Scientific Lab., Rep. No. 02-16, (Los Alamos National Laboratory, New Mexico, USA, 2002)
- [56] Hong-Yu Zhou, Fu-Guo Deng, Wei Cheng, *et al.*, *Nucl. Instrum. Methods Phys. Res. A* **648**(1), 192 (2011)
- [57] A. Negret, C. Borcea, D. Bucurescu, *et al.*, *Phys. Rev. C* **88**, 034604 (2013)
- [58] M. Boromiza, C. Borcea, P. Dessagne, *et al.*, *Phys. Rev. C* **101**, 024604 (2020)
- [59] A. P. Arya, D. L. Campbell, R. D. Wilson, *Bull. Am. Phys. Soc.* **12**, HD4 (1967)
- [60] W. Breunlich, G. Stengl, H. Vonach, *Z. Naturforsch. A* **26**, 451 (1971)
- [61] G. L. Morgan, D. C. Larson, The  $Ti(n, xy)$  reaction cross section for incident neutron energies between 0.3 and 20.0 MeV, Oak Ridge National Lab. technical memo, No.6323, (Oak Ridge National Laboratory, Oak Ridge, TN, USA, 1978); <https://inis.iaea.org/records/806kn-26t18>
- [62] D. Dashdorj, P. E. Garret, J. A. Becker, *et al.*, *AIP Conf. Proc.* **769**, 1035 (2005)
- [63] D. Dashdorj, G.E. Mitchell, J. A. Becker, *et al.*, *Nucl. Sci. Eng.* **157**(1), 65 (2007)
- [64] A. Olacel, F. Belloni, C. Borcea, *et al.*, *Phys. Rev. C* **96**, 014621 (2017)
- [65] H. O. M. Kinney, *Inelastic scattering of 14.4 MeV Neutrons from several elements*, Ph.D. Thesis (Morgentown: University of West Virginia, WV, USA, 1972).
- [66] F. Voss, S. Cierjacks, D. Erbe, G. Smalz, Measurement of the gamma-ray production cross section from inelastic neutron scattering in some chromium and nickel isotopes between 0.5 and 10 MeV, in *Proceedings of the Conference on Nuclear Cross Sections and Technology, Washington, USA, 1975*, edited by Roald A. Schrack, Charles D. Bowman, (USA: Department of Commerce, National Bureau of Standards, Institute for Basic Standards, Center for Radiation Research, 1975), Vol.2, p.916. <https://nvlpubs.nist.gov/nistpubs/Legacy/SP/nbsspecialpublication425v2.pdf>
- [67] T. Yamamoto, Y. Hino, S. Itagaki, *et al.*, *J. Nucl. Sci. Technol.* **15**(11), 11 (1978)
- [68] P. Oblozinsky, S. Hlavac, G. Maino, *et al.*, *Il Nuovo Cimento A* **105**, 965 (1992)
- [69] L.C. Mihailescu, C. Borcea, A.J. Koning, *et al.*, *Nucl. Phys. A* **786**(1-4), 1 (2007)
- [70] M. A. Bostrom, I. L. Morgan, J. T. Prud'homme, *et al.*, Interaction of fast neutrons in iron, lead, oxygen and hydrogen, Wright Air Devel. Centre Reports, Rep. No. 50-31, (Texas Nuclear Corp., Austin, TX, USA, 1959)
- [71] B. Joensson, K. Nyberg, I. Bergquist, *Ark. Foer Fys.* **39**, 295 (1969)
- [72] B. I. Sukhanov, N. P. Tkach, *Sov. J. Nucl. Phys.* **11**, 17 (1970)
- [73] A. P. Degtyarev, V. V. Kravtsov, A. Prokopets, Gamma-rays connected with the nonelastic processes of the deuterium-tritium neutrons on the nuclei Na, Fe, USSR report to the I.N.D.C., Rep. No. INDC(CCP)-118, (Kyivsky Natsionalny Univ. "Taras Shevchenko", Kyiv, Ukraine, 1977).
- [74] S. Xiamin, S. Ronglin, X. Jinqiang, W. Yongshun, and D. Dazhao, Measurements of the induced gamma ray cross-sections by 14.2 MeV neutrons with Fe, Ni and Cu, in *Proceedings of Conference on Nuclear Data for Science and Technology, held in Antwerpen, Belgium, 6-10 September 1982*, edited by K. H. Böckhoff, (Holland: D. Reidel Publishing Company, 1982), p. 373; <https://doi.org/10.1007/978-94-009-7099-1>
- [75] B. Al-Shalabi, A. J. Cox, *Nucl. Instrum. Methods Phys. Res.* **205**(3), 495 (1983)
- [76] S. Hlavac, P. Oblozinsky, Gamma-ray production cross sections and gamma-ray multiplicities from Fe and Ni bombarded with 14.6 MeV neutrons, CSR report to the INDC, Rep. No. INDC(CSR)-5 INT(83)-7, (IAEA NDS, Vienna, Austria, 1983); <https://www-nds.iaea.org/publications/indc/indc-csr-0005.pdf>
- [77] X. Jinqiang, C. Zhong, W. Yongshun, *et al.*, *Chin. J. of Nucl. Phys.* **10**(3), 284 (1988)
- [78] H. Sakane, Y. Kasugai, F. Maekawa, Y. Ikeda, and K. Kawade, "Measurement of discrete gamma-ray production cross sections for interaction of 14-MeV neutrons with Mg, Al, Si, Ti, Fe, Ni, Cu, Nb, Mo and Ta," in *Proceedings of the 1998 Symposium on Nuclear Data, held in Tokai, Japan, November 19-20 1998*, edited by Tadashi Yoshida and Tokio Fukahori, (Japan: Japan Atomic Energy Research Institute, 1999), p. 216; <https://inis.iaea.org/records/6t2mv-k9p62>
- [79] A. Negret, C. Borcea, Ph. Dessagne, *et al.*, *Phys. Rev. C* **90**, 034602 (2014)
- [80] D. L. Broder, A. F. Gamaliy, A. I. Lashuk, *et al.*, The  $(n, n'\gamma)$  reaction on Fluorine, Iron, Cobalt, Nickel and Tantalum, in *Proceedings of the Second International Conference on Nuclear Data for Reactors*, edited by IAEA editorial staff, (Austria: IAEA, 1970), Vol. 2, p. 295; <https://www-nds.iaea.org/publications/proceedings/sti-pub-259-Vol2.pdf>
- [81] G. T. Western, R. C. Baird, F. L. Gibbons, *et al.*, The interactions of 14.6-MeV neutrons in iron, Lithium-7, and carbon, Techn. Report, Rep. No.64-140, (General Dynamics, Fort Worth, USA 1965); <https://apps.dtic.mil/sti/html/tr/AD0614451/index.html>
- [82] M. Mitsuda, T. Kondo, I. Murata, *et al.*, *J. Nucl. Sci. Technol.* **39**(2), 437 (2002)
- [83] R. Antalík, S. Hlavac, P. Oblozinsky, in *Neutron induced reactions*, Vol. 6. (VEDA, Publishing House of the Slovak Academy of Sciences, 1980), p. 277.
- [84] R. O. Nelson, N. Fotiades, M. Devlin, *et al.*, *AIP Conf. Proc.* **769**(1), 838 (2005)
- [85] S. P. Simakov, A. Pavlik, H. Vonach, *et al.*, Status of experimental and evaluated discrete  $\gamma$ -rays production at  $E_n=14.5$  MeV, final report of research contract 7809/RB, performed under the CRP on measurement, Calculation and Evaluation of Photon Production Data, INDC(CCP)- 413, (IAEA NDS, Vienna, 1998); <https://inis.iaea.org/records/c44gw-yfn27>
- [86] E. P. Bogolyubov, A. V. Gavryuchenkov, M. D. Karetnikov, *et al.*, Neutron generators and DAQ system for tagged neutron technology, in *Proceedings of the XXVI International Symposium on Nuclear Electronics & Computing (NEC'2017), held in Becici, Budva, Montenegro, September 25 - 29, 2017* edited by Vladimir Korenkov and Andrey Nechaevskiy, (Russia: JINR, 2017) p. 176;

- [87] <https://ceur-ws.org/Vol-2023/176-181-paper-27.pdf>  
R. Capote, M. Herman, P. Oblozinsky, *et al.*, *Nucl. Data Sheets* **110**(12), 3107 (2009)
- [88] <https://www.nndc.bnl.gov/ensdf/>, Evaluated Nuclear Structure Data Files (ENSDF) database, retrieved 15th August 2025;
- [89] S. Agostinelli, J. Allison, K. Amako, *et al.*, *Nucl. Instrum. Methods Phys. Res. A* **506**(3), 250 (2003)
- [90] J. Allison, K. Amako, J. Apostolakis, *et al.*, *Nucl. Instrum. Methods Phys. Res. A* **835**, 186 (2016)
- [91] Richard M. Lindstrom, Richard B. Firestone, R. Paviotti-Corcuera, Development of a Database for Prompt  $\gamma$ -ray Neutron Activation Analysis, Summary Report of the Third Research Coordination Meeting (INDC(NDS)-443), (IAEA NDS, Vienna, Austria, 2003); [https://www-nds.iaea.org/pgaa/Annex1/INDC\\_NDS\\_443.pdf](https://www-nds.iaea.org/pgaa/Annex1/INDC_NDS_443.pdf)
- [92] A. Koning, S. Hilaire, S. Goriely, *Eur. Phys. J. A* **59**, 131 (2023)
- [93] D.A. Brown, M.B. Chadwick, R. Capote, *et al.*, *Nucl. Data Sheets* **148**, 1 (2018)
- [94] O. Iwamoto, N. Iwamoto, S. Kunieda, *et al.*, *J. Nucl. Sci. Technol.* **60**(1), 1 (2023)
- [95] A. Negret, M. Sin, C. Borcea, *et al.*, *Phys. Rev. C* **96**, 024620 (2017)
- [96] C.R. Brune, *Nucl. Instrum. Meth. Phys. Res. A* **493**, 106 (2002)